UNIVERSITY OF OKLAHOMA

GRADUATE COLLEGE

AN INTEGRATED PALEOMAGNETIC AND DIAGENETIC STUDY OF THE WOMBLE
SHALE IN THE BENTON UPLIFT, ARKANSAS

A THESIS

SUBMITTED TO THE GRADUATE FACULTY

in partial fulfillment of the requirements for the

Degree of

MASTER OF SCIENCE

By

ELIZABETH SMITH
Norman, Oklahoma
2021

AN INTEGRATED PALEOMAGNETIC AND DIAGENETIC STUDY OF THE WOMBLE
SHALE IN THE BENTON UPLIFT, ARKANSAS

A THESIS APPROVED FOR THE
MEWBOURNE COLLEGE OF EARTH AND ENERGY

BY THE COMMITTEE CONSISTING OF

Dr. R. Douglas Elmore, Chair

Dr. Shannon Dulin

Dr. Andrew S. Elwood Madden

Acknowledgements

Thank you to everyone who has made this journey and research possibly. I would like to thank Dr. Elmore for the continued support and encouragement for both academic and professional pursuits over the past two years. I greatly appreciate the guidance throughout this project. Thank you to my committee members, Dr. Dulin and Dr. Elwood Madden, for feedback on research. I would also like to thank all others who make this research possible – thank you to fellow graduate students for always providing motivation, academic guidance, and wonderful friendships, to undergraduate students who helped collect paleomagnetic data, and all other faculty members who I had the opportunity to learn from. I am also very grateful for the continuous support from my closest friends and family who have been by my side the entire time.

Table of Contents

List of Figures

characteristic remnant magnetization (ChRM) at higher field strengths. This paleomagnetic data

is displayed on a Zijderveld diagram which is an orthogonal projection that displays both

directional and intensity information. The blue points are the declination which represent

directions (N, S, E, W) and the red points are the apparent inclination which are tied to the

declination by a vertical line and represent (up and down directions). The units on both axis are

measured in milli amps per meter and intensity decreases moving towards the origin.

Components are magnetization which have a direction including inclination and declination and

Figure 18: Photomicrographs of the Womble Shale including the matrix, veining, and stylolites.

a) Matrix including quartz, calcite, albite, dolomite, and muscovite (XPL). b) Matrix and vein

with a stylolite that extends from the matrix and one branch appears to follow the left side of the

vein; stained with alizarin red (PPL). c) Large vein composed of twinned calcite and fractured

quartz (XPL). d) Authigenic grains of albite and hexagonal quartz located in the matrix with

Abstract

The objective of this project is to conduct an integrated paleomagnetic and diagenetic study of the Ordovician Womble Shale in Mt. Ida, Arkansas, in order to test if diagenetic events can be identified and dated with petrographic and paleomagnetic techniques. Significant hydrothermal alteration has been identified and dated in western Arkansas and the paleomagnetic analysis will test if a magnetization of similar age that was caused by hydrothermal fluids can be identified. Samples were collected from a Womble Shale outcrop, located west of Mt. Ida, Arkansas, which are composed of shale alternating with calcareous sandstone lenses that contain numerous veins filled with quartz and calcite. The samples were characterized based on thin section petrography and scanning electron microscopy (SEM), and a paragenetic sequence was determined. In addition to acquiring paleomagnetic data to determine the timing, anisotropy of magnetic susceptibility (AMS) data was collected to examine the petrofabrics and identify alteration.

The calcareous sandstones contain a complicated diagenetic history which includes precipitation of authigenic phases during multiple fluid events and deformation. The calcite and quartz veins, both vertical and horizontal, are interpreted to be hydrothermal and syntectonic in origin. Hydrothermal minerals including xenotime, monazite, biotite, and sphalerite are identified within veins and in the matrix as are hydrocarbons. Stylolites containing mics are present in the matrix and in larger veins. Fibrous clay bands composed predominantly of muscovite and illite with hematite staining are also present in the matrix. Diagenesis within the Womble Shale indicates a unit influenced by hydrothermal fluids, most likely in several episodes, low-grade metamorphism, and deformation.

AMS data suggests that the petrofabric of the Womble Shale is a composite fabric with influences from burial, tectonic, and diagenetic processes. Alternating field (AF) demagnetization identified a post tilting thermoviscous remanent magnetization (TVRM) held in magnetite with a Late Mississippian pole. The demagnetization paths are curved which suggest contamination with a modern viscous magnetization and the pole age is not considered reliable. A magnetic component removed during thermal demagnetization after AF treatment reveals a post tilting characteristic remnant magnetization (ChRM) held in hematite with a Late Pennsylvanian pole position. The ChRM is interpreted as a thermochemical remnant magnetization (TCRM) caused by precipitation of hematite during hydrothermal alteration. The petrographic and paleomagnetic results suggest the acquisition of a syntectonic hematite magnetization in the Late Pennsylvanian probably coincided with hydrothermal alteration. This contrasts with other studies which report post orogenic hydrothermal activity in the Ouachitas (e.g., Shelton et al., 1986).

1. Introduction

The purpose of this project is to contribute to the overall understanding of the paleomagnetic characteristics of shales, particularly the Ordovician Womble Shale in the Ouachita Mountains, as well as to characterize and date diagenetic events through paleomagnetic and petrographic techniques. A paleomagnetic analysis of the Womble Shale will test if a remagnetization is present. The age of remagnetization will be compared to a previous study which reported a date of 262 ± 10 Ma for hydrothermal alteration based on K-Ar dating (Shelton et al., 1986) in the Womble Shale. It will also be compared to a paleomagnetic study in southern Oklahoma which reported alteration by hydrothermal fluids at about 260 Ma (Roberts et al., 2019) in the Woodford Shale. These studies indicate the hydrothermal alteration was post orogenic and additional studies will help determine the distribution of this alteration and shed light on its origin. This study will also provide a test of the paleomagnetic dating approach compared with another method, K-Ar dating.

A diagenetic study will help to establish the paragenesis, identify magnetic and other authigenic minerals, and determine the relative timing of events. Understanding fluid alteration properties and the resulting authigenic phases is beneficial to our understanding of shales which can be diagenetically complex (e.g., Roberts et al., 2019). The investigation into the diagenetic properties of the unit will help characterize the relative timing of hydrothermal alteration.

The study area is located in the Benton Uplift of the Ouachita Mountains in Arkansas (Figure 1). The middle-upper Ordovician Womble Shale (Figure 2) is organic rich and is a potential unconventional reservoir although very little organic geochemical research has been conducted on the unit (e.g., Fowler, 1984). After a reconnaissance sampling and preliminary

paleomagnetic analysis, one outcrop composed of calcareous sandstone and shale became the

focus of the study (Figure 3).

2. Geologic Setting

The Womble Shale is an Ordovician-aged unit which outcrops primarily within the Benton and Broken Bow uplifts located in Arkansas and Oklahoma, respectively. The exposed outcrop in the Ouachita Mountains reveals a lithology of mostly dark shale with limestone and sandstone lenses as well as interbedded chert (Johnson, 1996). The Womble Shale is described as a black, carbonaceous, graptolitic shale with interbedded units of sandstone, limestone and phosphatic breccias (Buthman, 1985). Milky quartz veins are also present throughout the unit (Stone and Sterling, 1962). The Womble Shale is overlain by the Bigfork Chert and underlain by the Blakely Sandstone, also both Ordovician in age as shown in Figure 2 (Arbenz, 1989; McFarland, 1998). The Womble Shale ranges from 500 – 1000 feet in thickness (Stone and Bush, 1982). Deposition took place during times of rising and falling seas on a deep-water, off-shelf setting ranging from slope to abyssal plain (Arbenz, 1989). Deposition occurred by turbidites, pelagic fallout, and mass flow processes (Arbenz, 1989). The early Ouachita Basin has both deep-water turbidity current deposits deriving from exterior sources and pelagic and hemipelagic deposits (Glick et al., 1991).

During deposition of the Womble Shale, pre-flysch sediment was sourced from the south into the Ouachita Basin which was a narrow tough (Lowe, 1985). Flysch sedimentation occurred from the Mid-Mississippian to Mid-Pennsylvanian (Figure 1) which were early signs of orogenic uplift (Arbenz, 1989; Blythe et al., 1988). During the Pennsylvanian, the Ouachita orogeny took place resulting in mountain building that produced the Ouachita Mountains (Suneson, 1995). These areas are characterized by thrust faults and other faults as well as folds (Figure 3). The deformation took place over a 40-million-year time period. The antiformal structure on the Benton Uplift occurred when the Johns Valley normal fault system was reactivated causing

basement uplift (Blythe et al., 1988). Around 310 million years ago at the end of the orogeny, continued uplift and erosion resulted in exposure of the Broken Bow and Benton areas (Suneson, 1995). This was the final phase of the mountain building event which created the present day Ouachita Mountains.
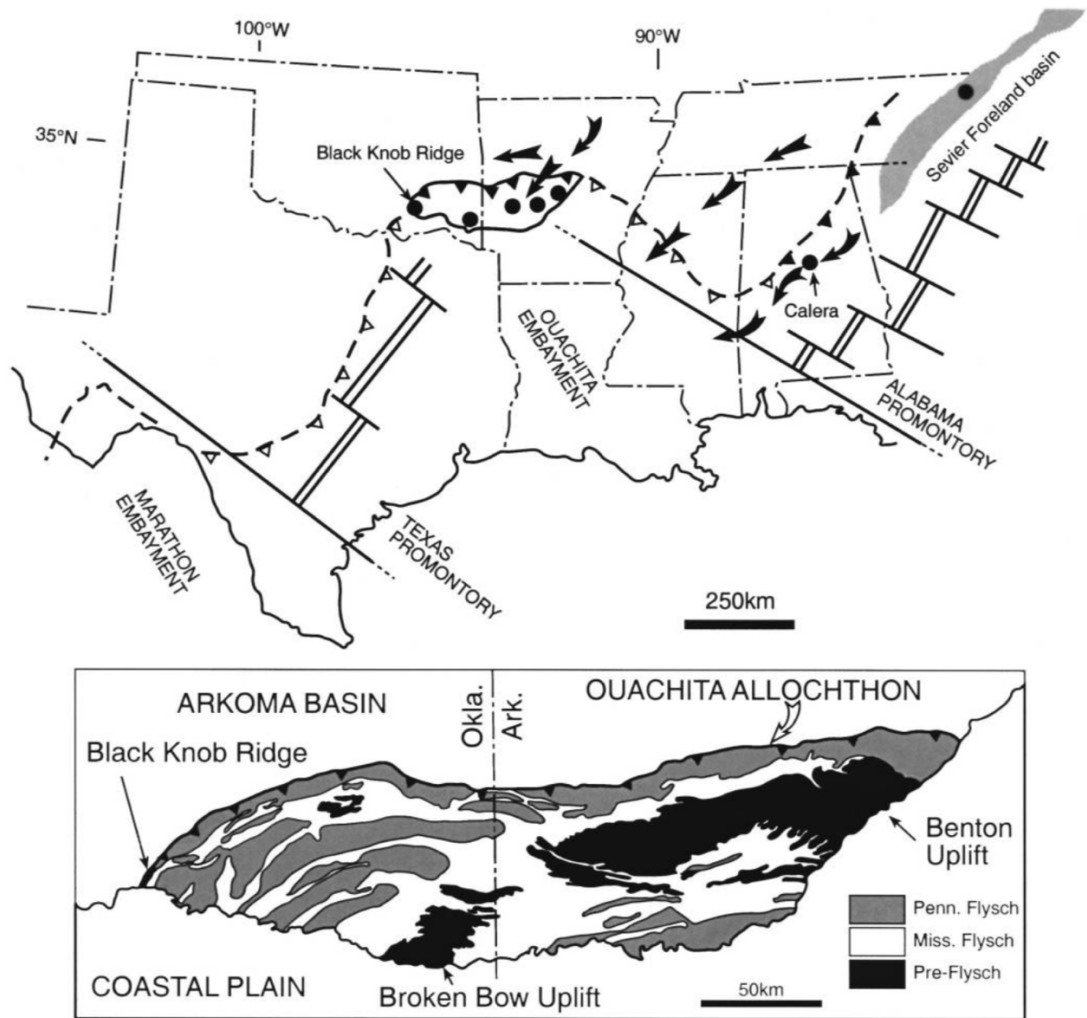
Figure 1: Rift margin and pre-flysch sedimentation of the Womble Shale within the Benton uplift (From Gleason et al., 2002, adapted form Thomas, 1991). The Womble Shale is interpreted to have pre-flysch sedimentation (Lowe, 1985).
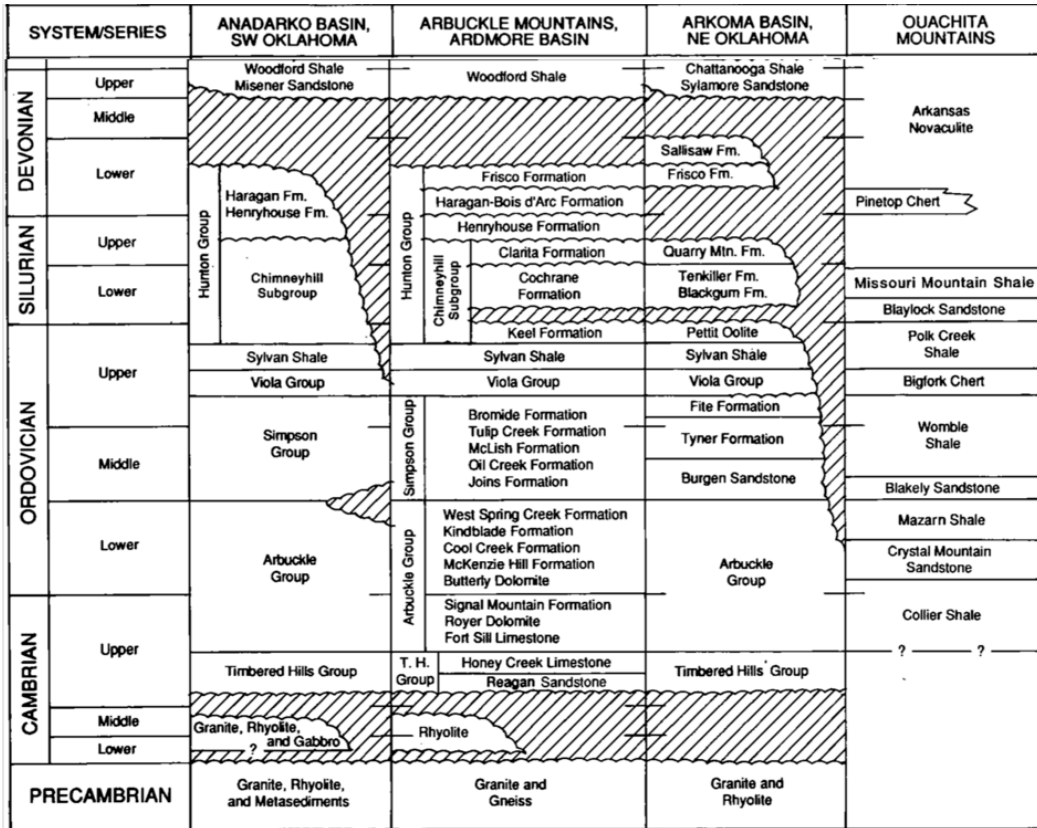
Figure 2: Sequence stratigraphy of Ouachita Mountains (from: Arbenz, 1989).

a)

N

A

34.36°

Maximum
Thickness

3300 m — Ms — Stanley Shale

290 m — MDa — Arkansas Novaculite

530 m — Smb — Missouri Mt Shale and Baylock Sandstone

250 m — Obf — Polk Creek Shale and Bigfork Chert

600 m — Ow — Womble Shale

150 m — Oby — Blakely Sandstone

900 m — Om — Mazarn Shale

250 m — Ocm — Crystal Mountain Sandstone

300 m — Oc — Collier Shale

Stratigraphic boundary

▲ ▲ Thrust Fault

■ ■ Normal Fault

5 km

Outcrop Mt. Ida

Lake Ouachita

397

270 Hot Spring →

27

Norman

Caddo Gap

A'

93.47'.30"

93.30'

34.22°

b)

Km
+2 A'-South

+1

0

-1

-2

-3

-4

-5

-6

Outcrop

A-North

Smb
Obf
Obf
Ow
Ocm Oc
Oby Ow
Om
Ow
Ocm
Oby
Om
Ocm
Oc
Om
Ow
Oby
Om
Ocm
Oc
Ow
Ow
Oby
Om
Ocm
Oc
Ms
MDa Smb
Ow Obf
Ocm

Figure 3: a) Geologic map of Mt. Ida, Arkansas with outcrop location (from: Chung, 2003) b) Geologic cross section from A-A' (from: Chung, 2003).

Hydrothermal quartz veins are present in the Womble Shale and formed towards the end of the Ouachita orogeny (Miser, 1959). Quartz veins extend for a length of 150 miles from the Broken Bow area of Southeast Oklahoma to Little Rock, Arkansas in a 30 to 40 miles wide band (Howard and Stone, 1988; Miser and Purdue, 1929). The hydrothermal veins are syntectonic and filled the fractures in thrust fault zones (Howard and Stone, 1988). Deformation of the Ouachita Mountains created complex vein fabrics and hydrothermal events altered the matrix. Shelton et al. (1986) dated adularia within the Womble Shale at 262 ± 10 Ma through K-Ar analysis and concluded that the adularia was deposited by hydrothermal fluids therefore constraining the age of postcollisional hydrothermal activity.

Post depositional deformation and low-grade metamorphism are both processes which also define the Benton uplift (Sutton and Land, 1996). Post depositional chemical alteration and low-grade metamorphism began during the late Paleozoic (Sutton and Land, 1996). Extended periods of diagenesis and metamorphism occurred in the Ouachita sequences after the relatively short folding and thrusting events with veining occurring towards the end of the deformation (Sutton and Land, 1996). A study by Johnson et al. in 2019 suggests that lower greenschist facies metamorphism occurred in the eastern Ouachitas because of high burial temperatures.

A study conducted by Gelason et al. 2002 analyzed the change in neodymium isotope composition at the Womble Shale/Bigfork Chert contact to better identify the source and timing of clastic sediment movement into the Ouachita region. This study used high-resolution graptolite-neodymium analysis and U-Pb dating of detrital zircon as a proxy for the source of the sediment and to estimate shifts in isotopic composition (Gleason et al., 2002). A change in isotope sediment composition took place over a 5-million-year time span due to local influences – first identified 457 Mya in the Eastern Ouachitas and 452 Mya in the Western Ouachitas

(Gleason et al., 2002). Sediments before the isotopic shift were sourced from the Archean Superior Province and the Grenville Province with minor amounts of sediment originating from the Granite-Rhyolite Terrane and Great Plains orogen (Gleason et al., 2002). After the isotopic shift, sediments were sourced primarily from the Grenville Province (Gleason et al., 2002). Although local variation in sediment source occurred, by 450 Mya well-mixed sediments originating from the Appalachian orogeny were the main source of clastic sediment for the Ouachitas (Gleason et al. 2002). Tectonics from the Appalachian-Taconian thrust belts combined with rising sea levels during the Ordovician produced isotopically uniform sediment which became the main source of clastic sediment for the Ouachita area (Gleason et al., 1994; Patchett et al., 1999).

3. Previous Work

Diagenetic analysis including reports of hydrothermal fluid activity and changes in metamorphism reaching greenschist facies have been recorded in the Benton uplift (Johnson et al., 2019). As previously mentioned, Shelton et al. (1986) documented a late Permian post-collisional hydrothermal event in Arkansas that recorded 300ºC temperature of the host rock based on conodont color alteration indices. Johnson et al. (2019) also reports temperatures that ranged from 200-300ºC based on illite crystallinity data from the same outcrop sampled in this study. This hydrothermal event produced many of the quartz veins located in western Arkansas including within the Benton uplift (Shelton et al., 1986). Hydrocarbons in the form of solid bitumen have been identified in the Womble Shale and are interpreted to have formed as a result of biodegradation and devolatilization of crude oil (Curiale and Harrison, 1982; Fowler and Douglas, 1984).

Previous studies also characterize variations of metamorphism and vitrinite reflectance in and between the Benton and Broken Bow Uplifts (e.g., Sutton and Land, 1996). Vitrinite reflectance values indicate regional variation in thermal maturity occurred across the Broken Bow and Benton uplifts as shown in Figure 4, with the highest temperatures observed in the eastern Ouachita Mountains (Figure 4; Sutton and Land, 1996). Vitrinite reflectance values at the sampling location for this study are between and 2 and 3 (Johnson et al., 2019). Sutton and Land (1996) also suggested that postdepositional chemical alteration occurred across both uplifts, but most significantly in higher grade exposures in the eastern Ouachitas. This caused removal of elements such as Ca, Mg, Fe, Si, Na, and K in the more altered parts of the eastern Ouachitas relative to less mobile elements such as Ti, Al, Zr, Cr, and Ni resulting in an increased weight percentage of aluminum oxides in higher grade areas (Sutton and Land, 1996).
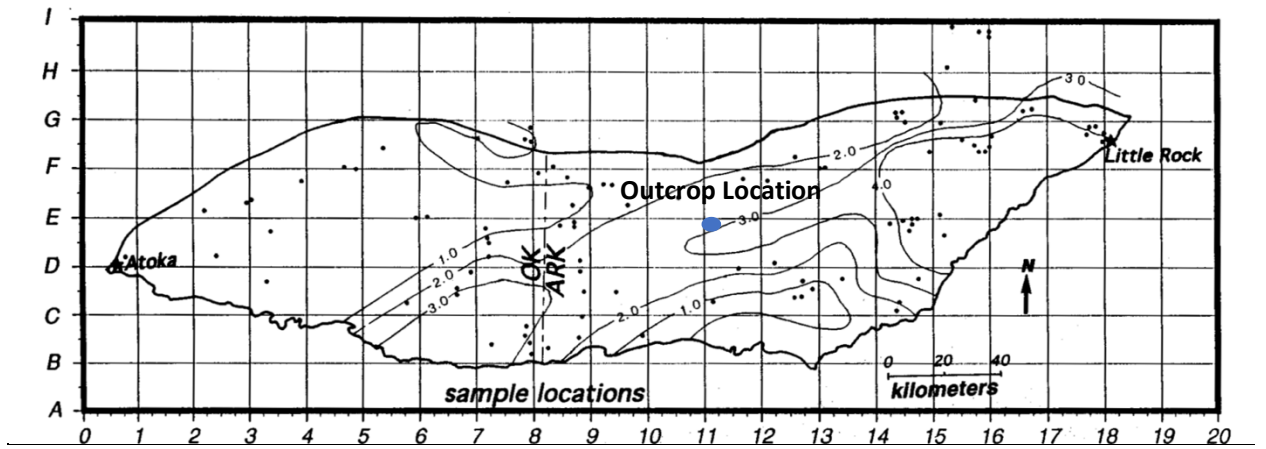
Figure 4: Vitrinite reflectance contours within the Benton and Broken Bow uplifts (from: Sutton and Land, 1996).

Chung (2003) characterizes the veins within the Womble Shale from the same outcrop location as the samples that are used in this study. He interpreted that veins were most likely formed by crystal growth exerting pressure along the fractures. Figure 5 is an image from Chung (2003) which illustrates the layers within the Womble Shale which consist of shale, calcareous sandstone, and different quartz and calcite vein types. Based on isotopic results (Chung, 2003), the fibrous veins, typical for greenschist facies metamorphism, as well as other veins, were formed by fluids in equilibrium with calcareous sandstone and host rock as opposed to externally derived fluids from different rocks (Chung, 2003).

The three types of veins and their orientations are characterized by Chung (2003): 1) thin (1-5 mm thick) calcite and quartz veins-in-shale (N68 E) which are finely fibrous 2), thin (1-5 mm thick) fibrous quartz and calcite veins (N45E) which originate in predominantly coarse-grained beds, and 3) thicker (5-30 mm) blocky quartz and calcite veins (N7E) which are typically located in calcareous sandstone layers. Chung (2003) also proposed the order of events which created the different types of veins and their compositions. In the first stage, fractures of tectonic origin start to form in a calcite rich unit while the shale layers are more ductile and do not fracture. In the second stage, uplift caused the shale layers to fracture and evidence of further stress such as stylolites formed. In the third stage, the phases in the veins were derived from the calcite rich layers and form the blocky quartz and calcite veins within the calcareous sandstone layers. Similar carbon and oxygen isotope values within all the veins and the calcite-rich calcareous sandstone layers, support that the veins material originated in calcite-rich layers and migrated to the calcareous sandstone and shale units (Chung, 2003) and were not derived from external fluids.

Figure 5: Layers and veins at the outcrop location (from: Chung, 2003).

The quartz veins within calcareous sandstone are proposed to be syntectonic, forming during the Ouachita orogeny. The calcite veins within shale most likely formed after the quartz veins and during uplift (Chung, 2003). Stylolites are also connected to veins and serve as conduits for material within the host rock. Stylolites most likely sourced components such as calcium which were unable to migrate through a shale matrix (Chung, 2003). Chung (2003) also suggests that calcite-rich lenses within the Womble Shale are the source of all the vein material. The presence of stylolites indicates that tectonic stress was present and caused dissolution of calcite which migrated to open fractures (Chung, 2003). Stylolites only served as dissolution sites for calcite in calcareous sandstone and conduits for calcite migration within shales units (Chung, 2003).

A previous paleomagnetic study in the Benton uplift focused on rotation of structural blocks but only included a few samples with poorly defined magnetizations from the Womble Shale (Smith and Jenkins, 1984). A previous study of the Bigfork Chert near Atoka in southern Oklahoma identified a chemical remnant magnetization (CRM) which was interpreted to be related to hydrothermal or orogenic fluids (Hillegeist et al., 1992). Roberts et al. (2019) conducted a paleomagnetic and diagenetic study of an oriented core in the eastern Ardmore Basin in southern Oklahoma and reported alteration by hydrothermal fluids at about 260 Ma. As previously stated, Shelton et al. (1986) reported a date of 262 ± 10 Ma for hydrothermal alteration in the Womble Shale. Adularia dating was also used by Bass and Ferrara (1969) which dated the veins at 287-279 Ma (Rb-Sr) and 214-190 Ma (K-Ar). Piper (2011) also used isotopic analysis, quartz-calcite oxygen isotope thermometry and fluid inclusion data to constrain vein formation from 300 to 315 Ma.

4. Methods

4.1 Sample Collection

During a reconnaissance sampling, samples of different lithologies (sandstone, shale, calcareous sandstone) were collected from 10 locations. Based on paleomagnetic analysis, the samples from one calcareous sandstone outcrop produced good results (described below) and that outcrop became the focus of the study. The samples of shale and sandstone from the other locations had weak or unstable magnetizations and no further analysis was conducted.

The sampled outcrop of the Womble Shale is located west of Mt. Ida, Arkansas on AR-379 or Southfork Road as shown in Figure 6. For the "379RC" samples, rock slabs were collected from the outcrop and a drill press was used to obtain cores. These cores were then oriented based off of original rock slab measurements from the field. The "SF1" and "SF2" samples were drilled in the field in order to obtain cores directly from the outcrop. Calcareous sandstone layers with veining were targeted when drilling for cores. These layers were drilled and cored parallel to the bedding plane and oriented in the field. 11 cores were obtained from the "379RC" slabs, 8 cores were obtained in the field from "SF1", and 12 cores were obtained in the field from "SF2". Cores from both the "379RC" site and "SF" sites were then cut down to standard 1-inch diameter plugs. Fifty-nine total calcareous sandstone plugs were produced from both the "379RC" and "SF" sites and used for both paleomagnetic, anisotropy of magnetic susceptibly (AMS), and petrographic studies.

Figure 6: Womble Shale outcrop located on AR-379 or Southfork Road, west of Mt. Ida, Arkansas.

4.2 Paleomagnetic and Anisotropy of Magnetic Susceptibility (AMS) Methods

All fifty-nine plugs were marked with "up" arrows indicating the depositional up direction of the plug and an Agico Kappa Bridge was used in order to measure the anisotropy of magnetic susceptibly (AMS). These measurements were taken in order to record the magnetic fabric of the cores. AMS data was plotted on a geographic equal area stereoplot to display results.

A 2G-Enterprise cryogenic magnetometer was used to measure the natural remnant magnetization (NRM) of all samples before they were subjected to several different demagnetization processes. Alternating field (AF) demagnetization was tested on twenty-three samples using a 2G Automated Degaussing system. AF demagnetization was conducted by

exposing samples from 10 mT up to a 120 mT (millitesla) alternating field which was completed by increasing alternating field in increments of 10 mT. After each exposure to the increased alternating field, the sample's magnetization was measured in the magnetometer.

Thermal demagnetization was conducted on two 379RC samples with twelve steps from 50ºC to 500ºC. Twenty-six more samples from SF1 and SF2 were thermally demagnetized from 50ºC to 400ºC over twelve steps. All demagnetization data was analyzed using Super IAPD2000 software. Rock magnetic studies including AF and thermal demagnetization help to confirm magnetic mineralogy by isolating components. Components are magnetizations which have a direction (inclination an declination) and they are identified as a straight line segment on Zijderveld (1967) diagrams with at least four demagnetization steps. The components are selected using principal component analysis (Kirschvink, 1980) with mean angle of deviations (MAD) less than 10°. Fischer (1953) statistics were used to determine mean directions. The age of magnetization is determined by plotting the pole position for the magnetization on an apparent polar wander path to determine the timing of magnetization (Torsvik et al., 2012).

Low temperature demagnetization (LTD) was conducted on two samples from SF1 and SF2 samples. The specimens were originally measured for NRM and then submerged in liquid nitrogen within a magnetic shield for approximately one hour. The specimens were measured for a NRM again. Specimens were then submerged and measured for NRM four more times for a total of five runs and six NRM measurements. Representative specimens were subjected to up to five LTD steps in liquid nitrogen and warmed in a zero field shield to remove a magnetization held in multidomain (MD) magnetite (Dunlop and Argyle, 1991; Warnock et al., 2000). Appendix 1 lists all fifty-nine plugs and what demagnetization techniques they were subjected to.

Isothermal remnant magnetization (IRM) experiments were conducted on two specimens to identify the magnetic mineralogy (Lowrie, 1990). Initially, specimens were subjected to AF demagnetization and then exposed to a fifty-five step acquisition processes from $10 - 2500$ mT. The specimens are subjected to an increasing IRM. An IRM was imparted with an ASC Scientific Impulse Magnetizer. Magnetic mineraologies were then identified by examining the shape of the curves when intensity was plotted versus mT on a graph. If the intensity increases at lower mT values (<100mT) then the mineral is a low coercivity mineral such as magnetite. If the curves continue to rise at higher mT values, then a high coercivity mineral such as hematite is present.

4.3 Petrographic Methods

Thin section analysis helps determine the paragenetic sequence by identifying the authigenic phases and providing insight on relative timing of diagenetic events based on textural relationships. Detrital and authigenic phases as well as relationships between veins, stylolites, and the rock matrix were analyzed. Twelve 379RC samples and ten SF samples were picked in order to analyze twenty-two thin sections. Thin sections were initially analyzed on a polarizing light microscope. Quartz and calcite veining within the calcareous sandstone was analyzed by staining several thin sections with an Alizarin Red solution. Several thin sections were selected to be analyzed by a scanning electron microprobe (SEM) and energy dispersive x-ray spectroscopy (EDS) in order to further aid in diagenetic mineral identification and provide a more detailed view of authigenic phases. A paragenetic sequence was produced from the petrographic work. Comparing the petrographic and paleomagnetic results was used to determine the origin of the magnetization.

5. Results and Interpretations

5.1 Anisotropy of Magnetic Susceptibility (AMS)

Anisotropy of magnetic susceptibility (AMS) data was collected for the three sites (SF1, SF2, and 379RC) within the same outcrop of the Womble Shale located west of Mt. Ida. AMS depicts the preferred orientation of magnetic minerals within a rock. The magnetic susceptibility can be represented as an ellipsoid with three principle susceptibility axes which are K1 as the maximum, K2 as the intermediate, and K3 as the minimum. AMS for the Womble Shale revealed a variety of different fabrics among the three sites including prolate to oblate, oblate, and triaxial.

A geographic equal area plot for SF1 from 17 samples shows a prolate to oblate rock fabric (Figure 7). The plugs obtained from SF1 are on average more heavily veined with diamagnetic quartz and calcite minerals than the other sites but all three sites contain both quartz and calcite-filled horizontal and vertical veins. The data for K2 and K3 is streaked with shallow inclinations and variable declinations. This and the two groupings of K1 in SF1 could be a result of a diagenetic fabric or a composite fabric including a primary and tectonic fabric. The east-west grouping of K1 would indicate a tectonic fabric. A geographic equal area plot for SF2 from 34 samples shows a triaxial rock fabric (Figure 8). The highlighted sample is sample SF2-8A which is composed entirely of quartz and calcite minerals from one vein. A geographic equal area plot for 379RC from 8 samples shows a dominantly prolate rock fabric resembling SF1 (Figure 9).

All AMS site data was compared to the N-S trending vein orientations produced by Chung (2003), however, no correlation between orientations were found. In general, the more heavily veined specimens have an oblate to prolate fabric while the less veined specimens have a

triaxial fabric. In summary, the AMS results suggest that the three sites contain a composite

fabric with contributions from a burial (close to vertical K3), a tectonic, and a diagenetic

processes.
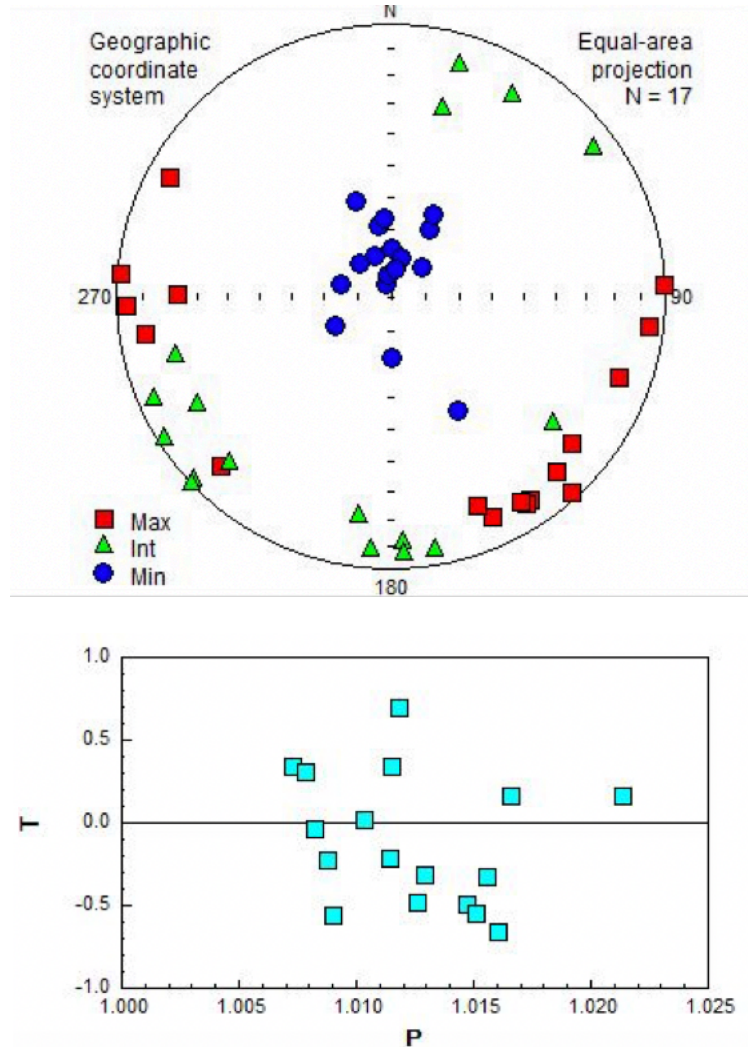
Figure 7: Geographic equal area plot for SF1 with a prolate to oblate rock fabric. The lower
figure is a Jelenk diagram (shape factor (T) versus the degree of anisotropy (P) which indicates
an oblate fabric if specimens are plotted above the center line and a prolate fabric if specimens
are plotted below the center line). Since specimens are for the most part equally distributed
above and below the line, this fabric is interpreted as prolate to oblate.
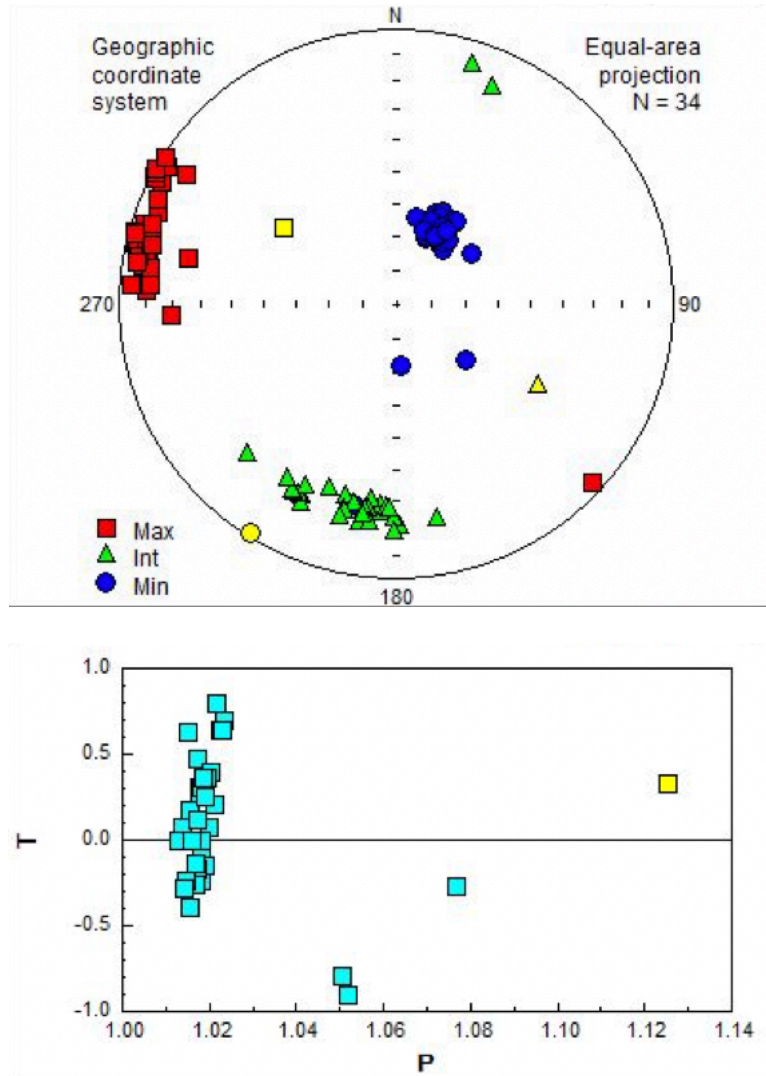
Figure 8: Geographic equal area plot of SF2 with sample SF2-8A highlighted in yellow. SF2 shows a triaxial rock fabric and the highlighted sample is composed entirely of diamagnetic minerals such as quartz and calcite.

21
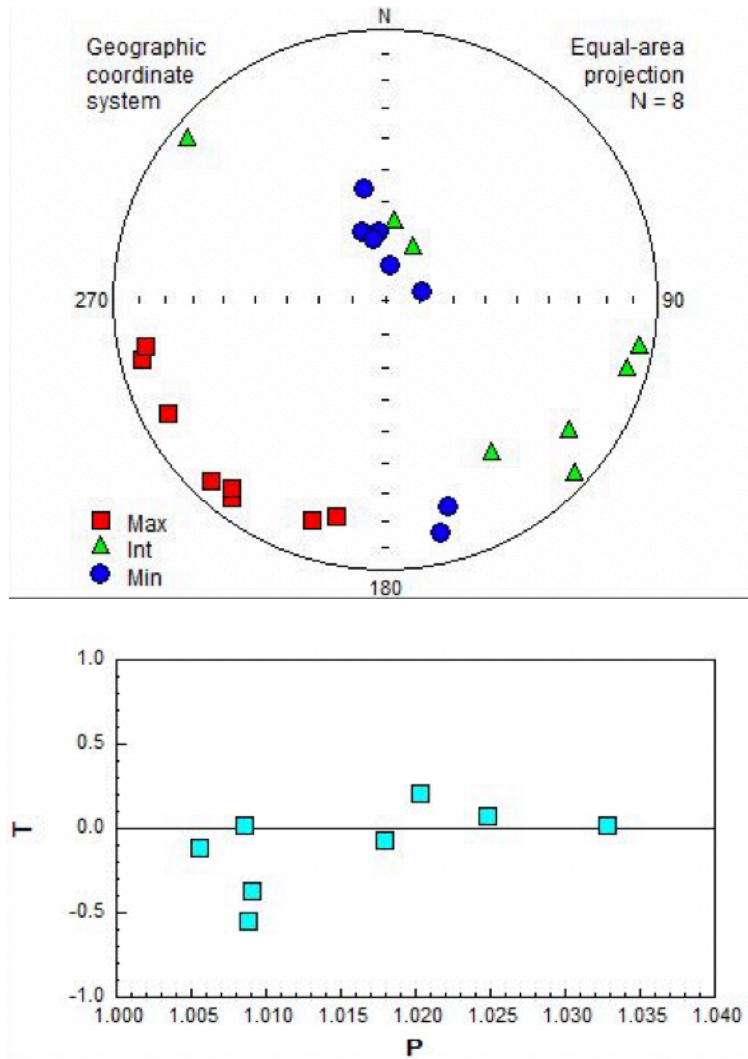
Figure 9: Geographic equal area plot of 379RC with a variable rock fabric.

5.2 Paleomagnetism

Specimens form 379RC, SF1, and SF2 were all used for paleomagnetic tests. Twenty-two specimens subjected to alternating field (AF) demagnetization isolated a component at low field strengths (NRM – 20 mT) with northerly declinations and steep down inclinations (Figure 10) interpreted as a modern viscous remnant magnetization (VRM). At higher fields strengths (20 – 120 mT) a component with southeasterly declinations and moderate inclinations is removed but significant magnetization remained after the AF treatment (Figure 10). The demagnetization path is also curved and the directions suggest a vector addition between the modern VRM and a southeasterly and shallow characteristic remnant magnetization (ChRM). As a result, the components were selected from high AF strengths (70 – 120 mT) to reduce the effects of the "curve" or contamination from the modern VRM. Although the average MAD (maximum angular deviation) angle is below 5º for all specimens, there was still a curve at high field strengths. The grouping of directions is good with a high grouping value (k > 20) and a low a95 (<10 º) (Figure 11) with a geographic mean at dec = 143.6º incl = 37.8º (k [grouping parameter, Fisher, 1953] = 113.2, a95 = 2.9º). The stratigraphic mean is dec = 128.5º incl = 48.5º (k = 65.8, a95 = 3º). Based on slightly different bed dips (SF1 dip = 8N; SF2 dip = 24N), the best grouping of the direction suggests it is a post tilting magnetization. There was no difference in the demagnetization results based on the abundance of veining present in specimens.
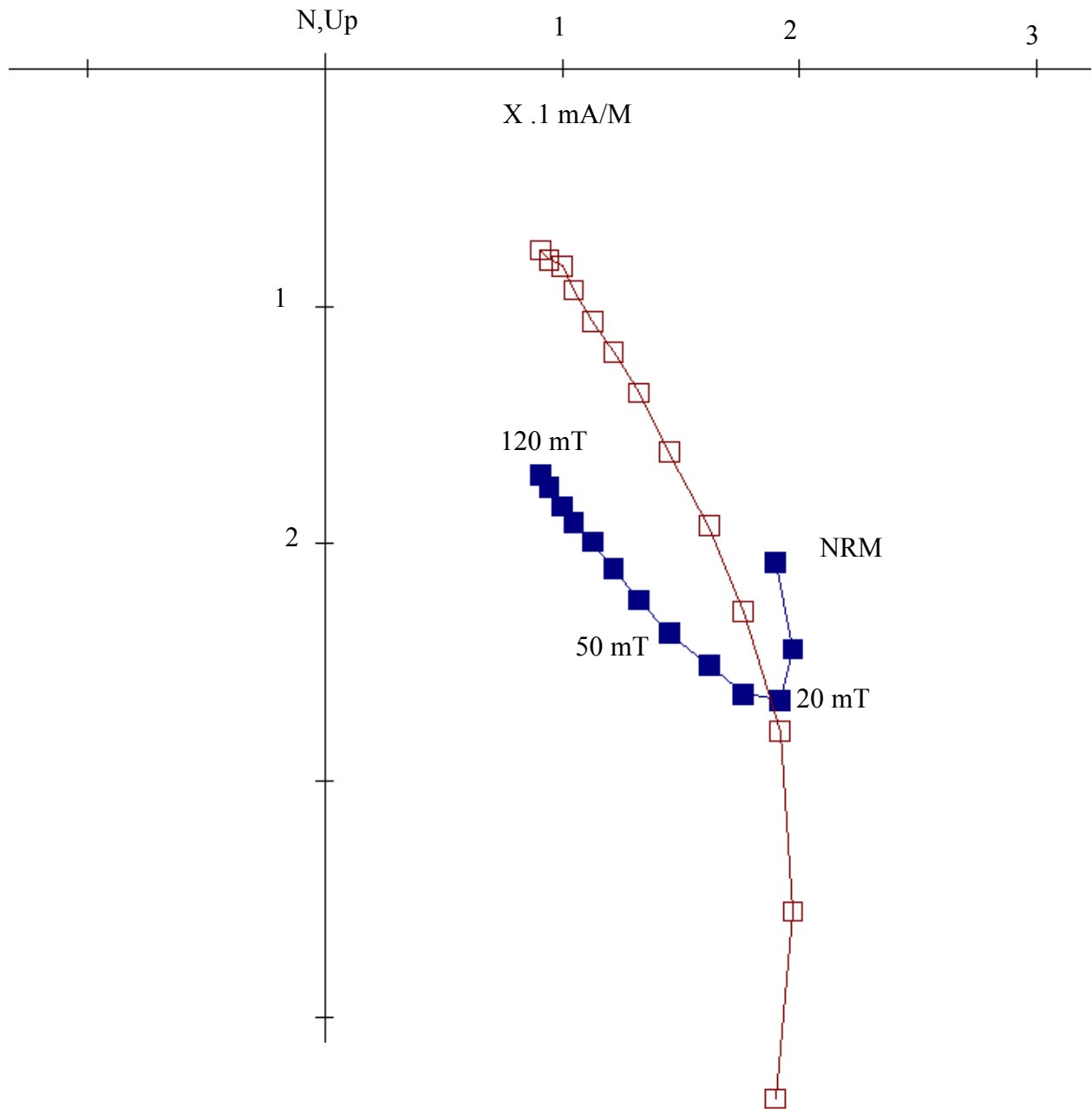
Figure 10: Alternating field Zijderveld (1967) diagram for a 379RC specimen with two interpreted components: a modern VRM at low field strengths and a southeasterly and shallow characteristic remnant magnetization (ChRM) at higher field strengths. This paleomagnetic data is displayed on a Zijderveld diagram which is an orthogonal projection that displays both directional and intensity information. The blue points are the declination which represent directions (N, S, E, W) and the red points are the apparent inclination which are tied to the declination by a vertical line and represent (up and down directions). The units on both axis are measured in milli amp per meter and intensity decreases moving towards the origin. Components are magnetization which have a direction including inclination and declination and they are identified as a straight line segment with at least 4 demagnetization steps.
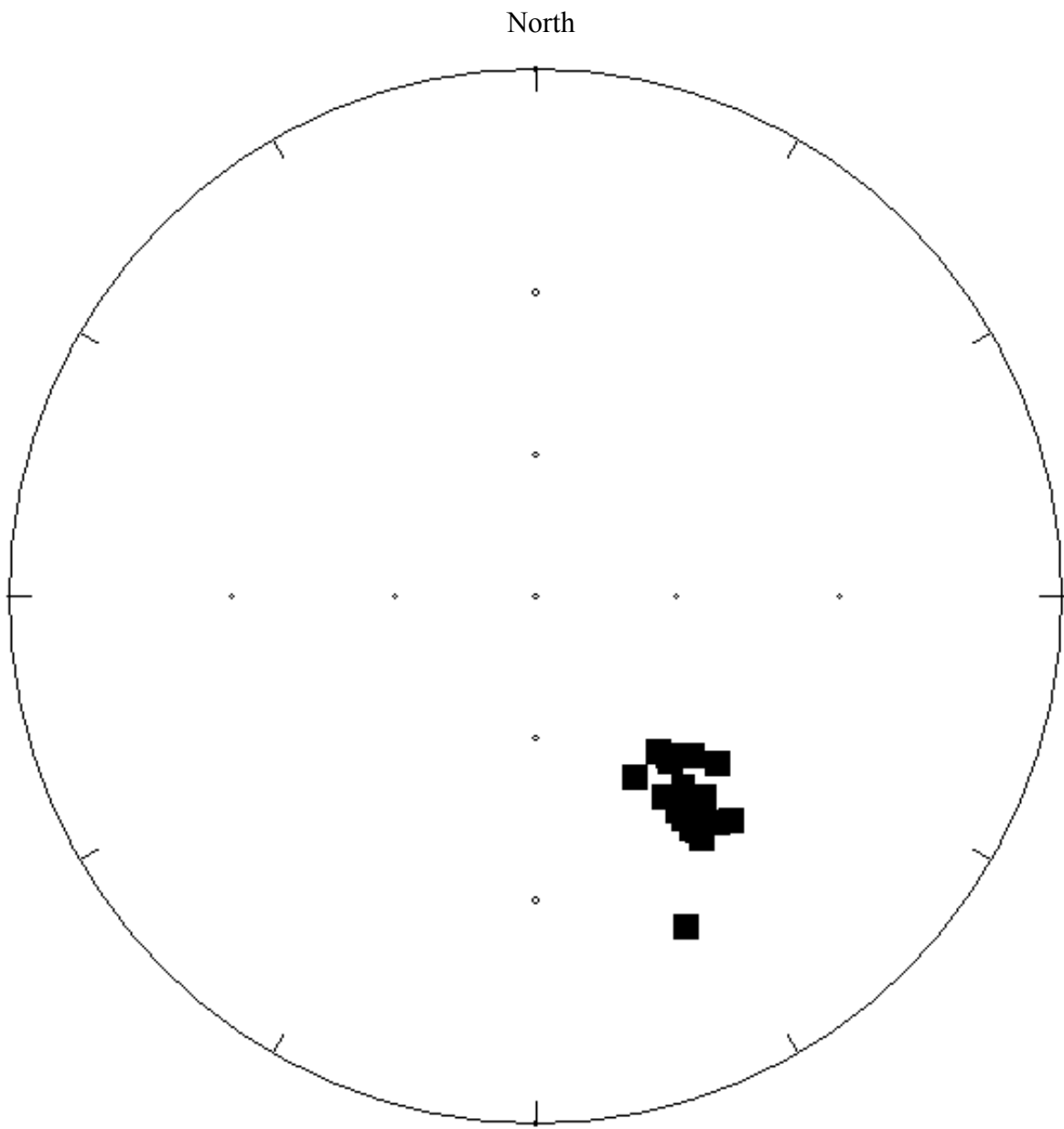
Figure 11: Equal area plot showing grouping of components removed by AF demagnetization.

Because of the possibility of contamination by a modern VRM in multidomain magnetite, several specimens were subjected to a five-step low temperature demagnetization (LTD) process (e.g., Dunlop and Argyle, 1991; Warnock et al., 2000). The LTD did not remove significant magnetization (7% average decrease in intensity) or isolate a component from the specimens.

Twin specimens from the same cores that were previously treated by AF demagnetization and LTD, as well as specimens not previously demagnetized, were subjected to thermal demagnetization. In specimens not previously demagnetized, thermal demagnetization removed a northerly and down characteristic remnant magnetization (ChRM) at low temperatures and then a component in a moderate-shallow and southeasterly direction at higher temperatures (Figure 12a). The magnetization shows a slight decrease in intensity below 275ºC and then a rapid decrease from 275-400ºC (Figure 12b).

In specimens previously treated by LTD and AF, thermal demagnetization removed the southeasterly and moderate to shallow component (Figure 13a, 14) during thermal demagnetization. The VRM is not present because it was removed by AF treatment. All MAD angles except for one specimen were below 5º for the thermal demagnetization components. Intensities began to decrease during thermal demagnetization around 275ºC and most of the magnetization is lost by 325ºC although linear decay extends up to 400ºC (Figure 13a and b). Above 400ºC the magnetic intensities in some specimens began to increase because of the creation of new magnetic minerals.

The grouping of directions is good for the component removed by thermal demagnetization (Figure 15) in geographic coordinates with a mean at dec = 152.4º incl = 14.3º (k = 268.1, a95 =1.9º). The stratigraphic mean is dec = 147.3º incl = 27.7º (k = 102.8, a95 = 2.9º). Based on slightly different dips, the best grouping of the directions suggest it is post tilting

magnetization. The k in geographic coordinates is 268.1 and the k post tilting is 102.8. The component isolated by thermal demagnetization has a shallower inclination than the component revealed by AF demagnetization (compare figures 11 and 14; Figure 15). Contamination of the AF component by a modern component most likely occurred (e.g., McCabe et al., 1984), accounting for the differences between the two components.
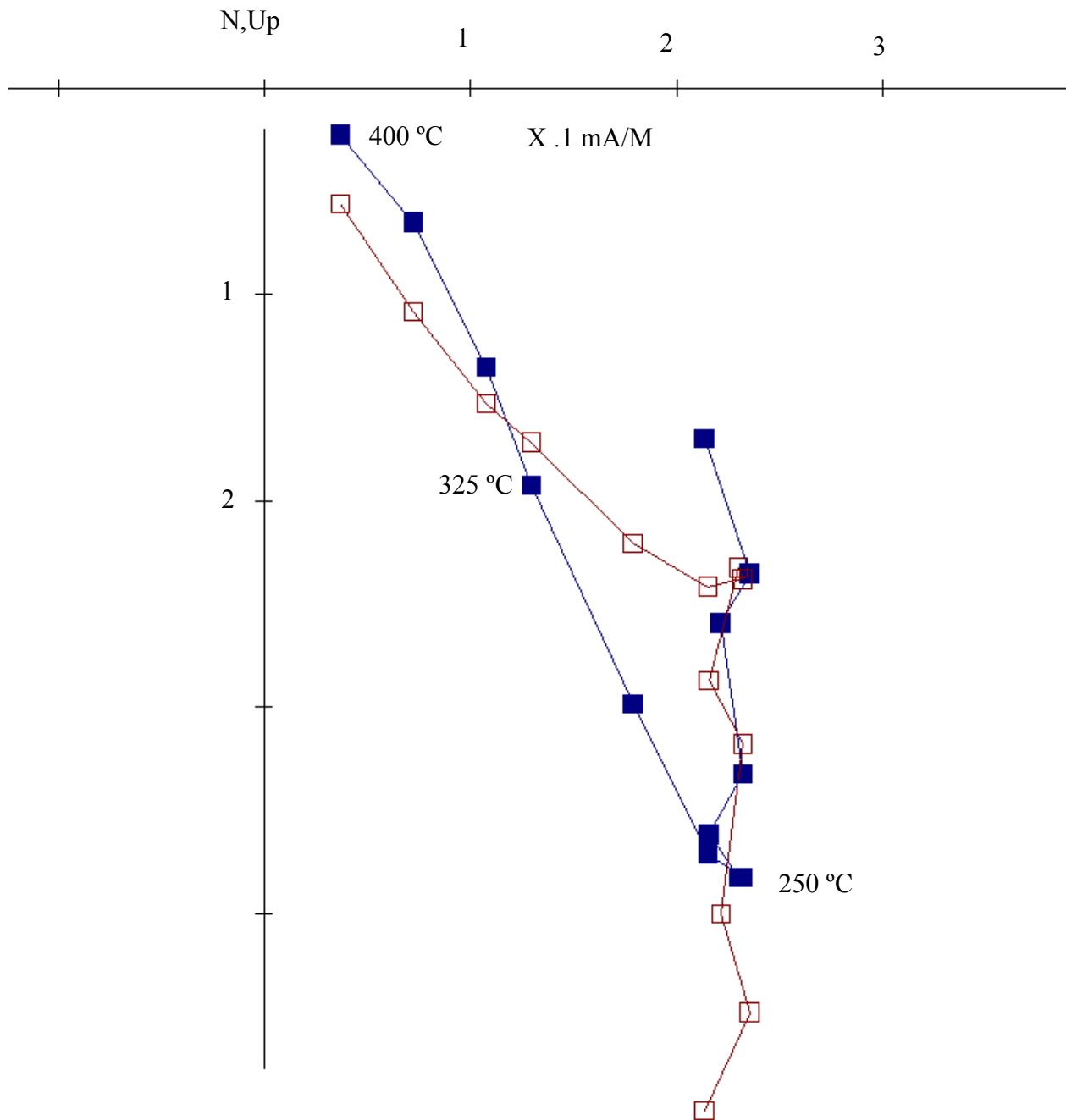
Figure 12a: Thermal demagnetization Zijderveld (1967) diagram for specimen not previously treated with AF.
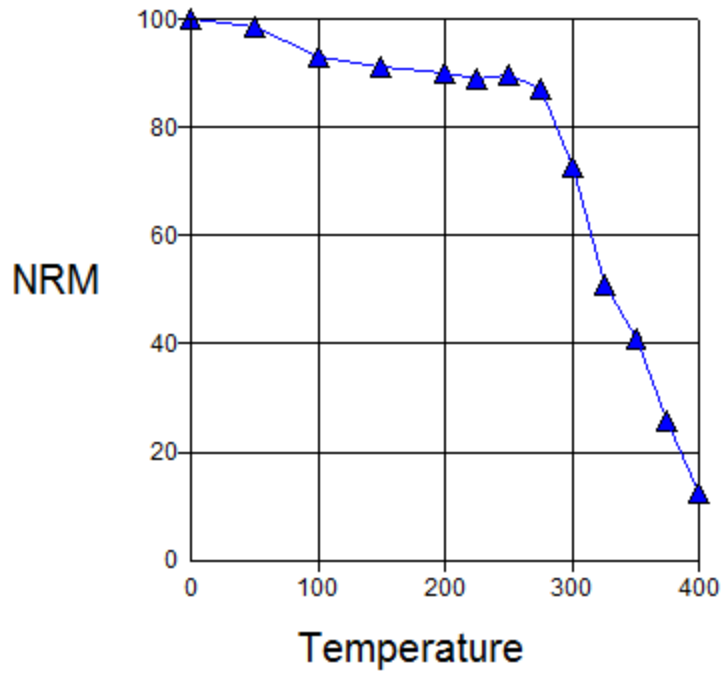
Figure 12b: Intensities versus temperature during thermal demagnetization. Specimen not previously treated with AF.
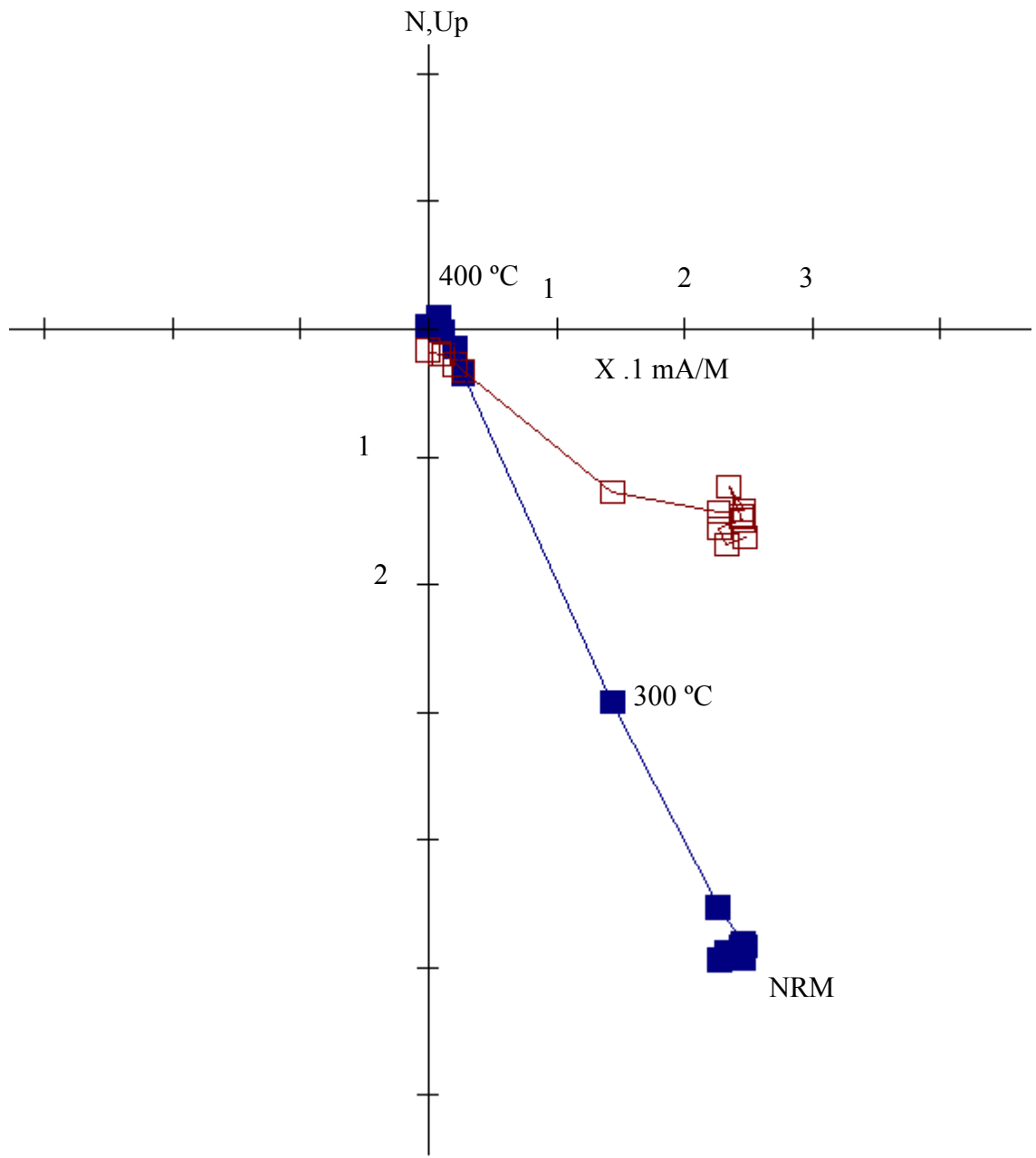
Figure 13a: Thermal demagnetization Zijderveld (1967) diagram for specimen previously treated with AF.
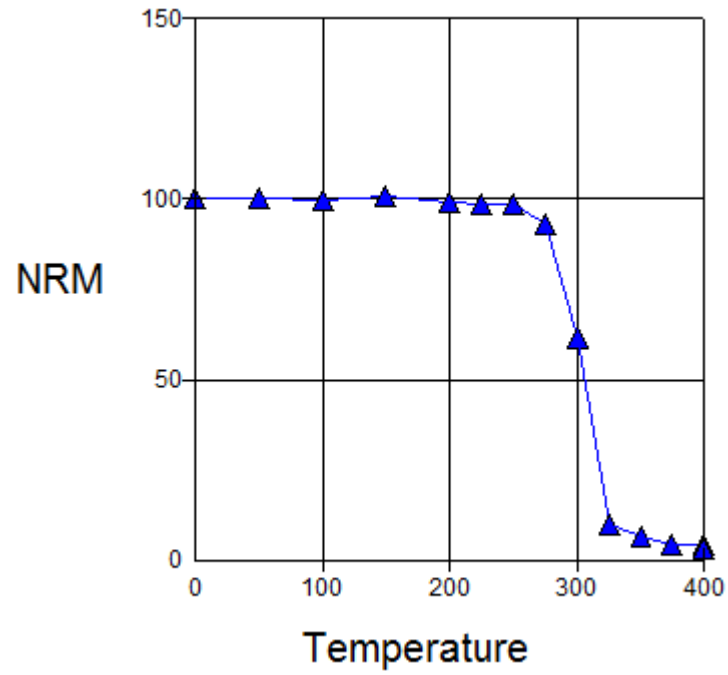
Figure 13b: Intensities measured on temperature steps during thermal demagnetization.
Specimen previously treated with AF.
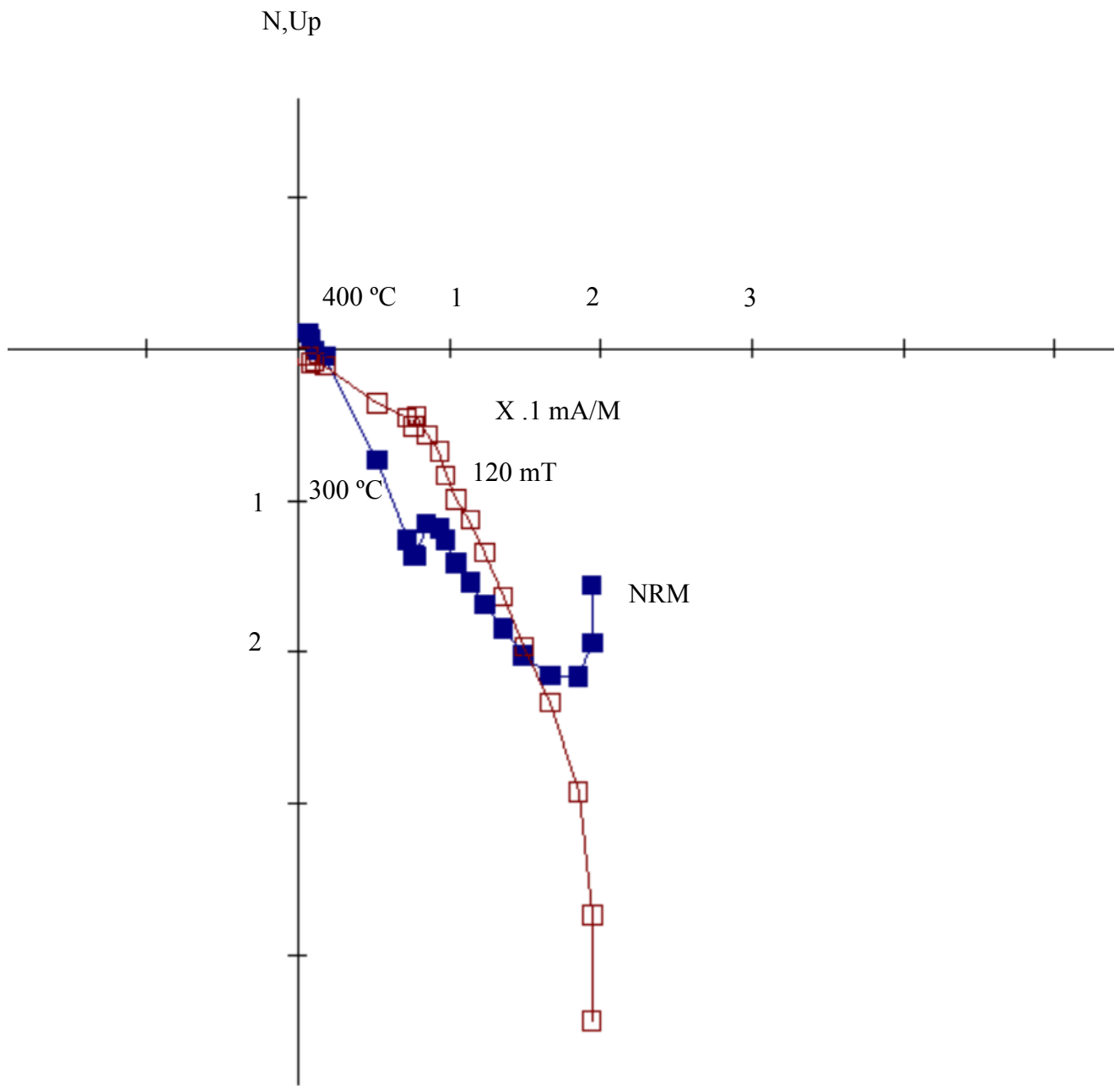
Figure 14: AF (10-120 mT) and thermal demagnetization (50-400ºC).
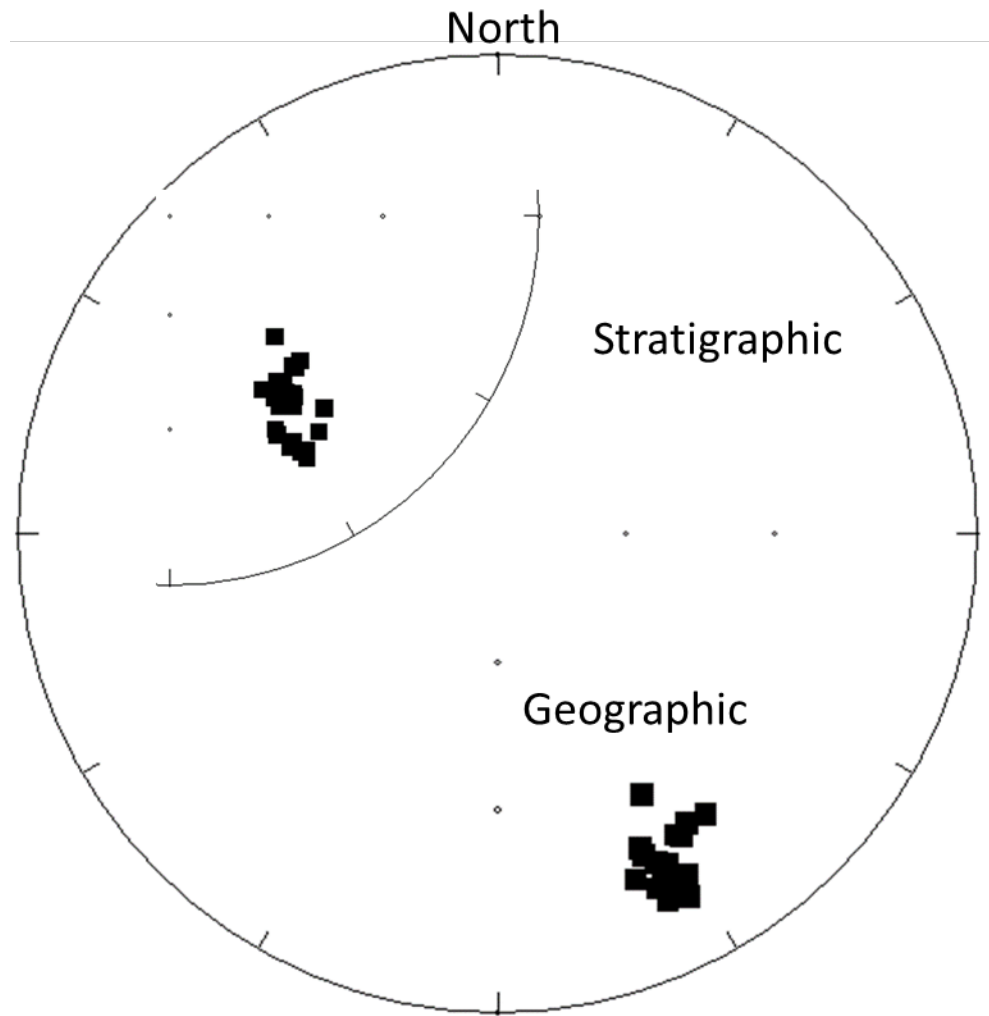
Figure 15: Equal area plot showing grouping of components from thermal demagnetization in geographic coordinates. Inset map shows directions in stratigraphic coordinates.

A geographic virtual geomagnetic pole (VGP) for AF demagnetization (24.4°N, 124.6°E, Dp = 2°, Dm = 3.4°) and thermal demagnetization (40.7°N, 123.7°E, Dp = 1°, Dm = 1.9°) are plotted on an apparent polar wander path (APWP) for North America (Figure 16). The AF demagnetization pole plots to the right of the path at an age of around 325 Ma consistent with a Late Mississippian age. The thermal demagnetization pole plots around 300 Ma consistent with a Late Pennsylvanian age. Because of the contamination issue, the pole and the age for the AF component should be viewed with caution.
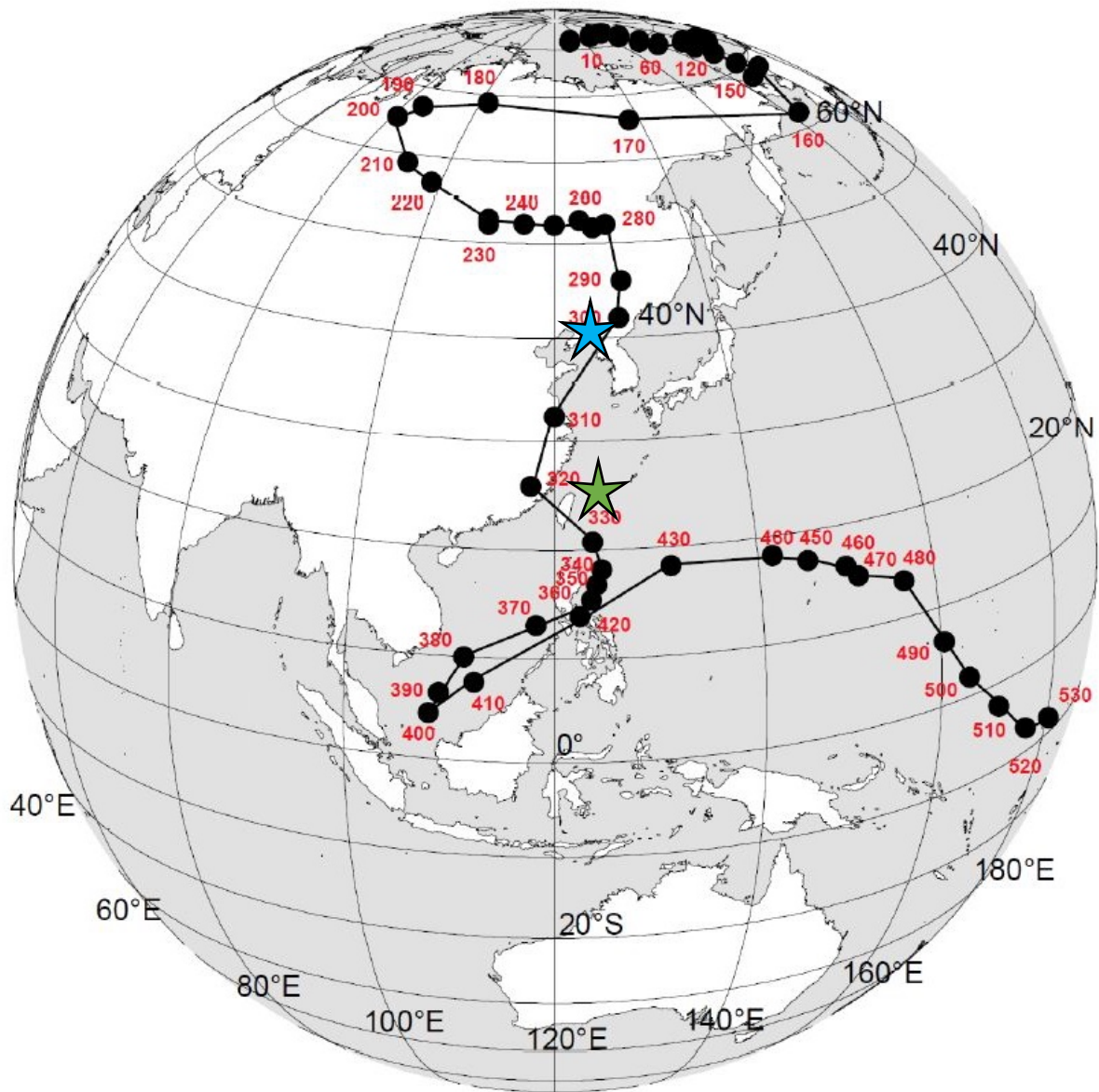
Figure 16: APWP showing two plotted components; pole plot from Torsvik et al. (2012):

★ AF demagnetization plot

★ Thermal demagnetization plot

Isothermal remnant magnetization (IRM) experiments (Lowrie, 1990) were performed to identify the magnetic mineralogy (Figure 17). The IRM curves show a rapid rise in intensity below 300 mT suggesting the magnetization is held in magnetite, and a gradual increase in intensity above 300 mT indicating a magnetization is held in high coercivity hematite. These results are consistent with the demagnetization results. The component removed by AF demagnetization is interpreted to reside in magnetite while the ChRM in specimens that were thermally demagnetized after AF treatment are interpreted to reside in hematite.
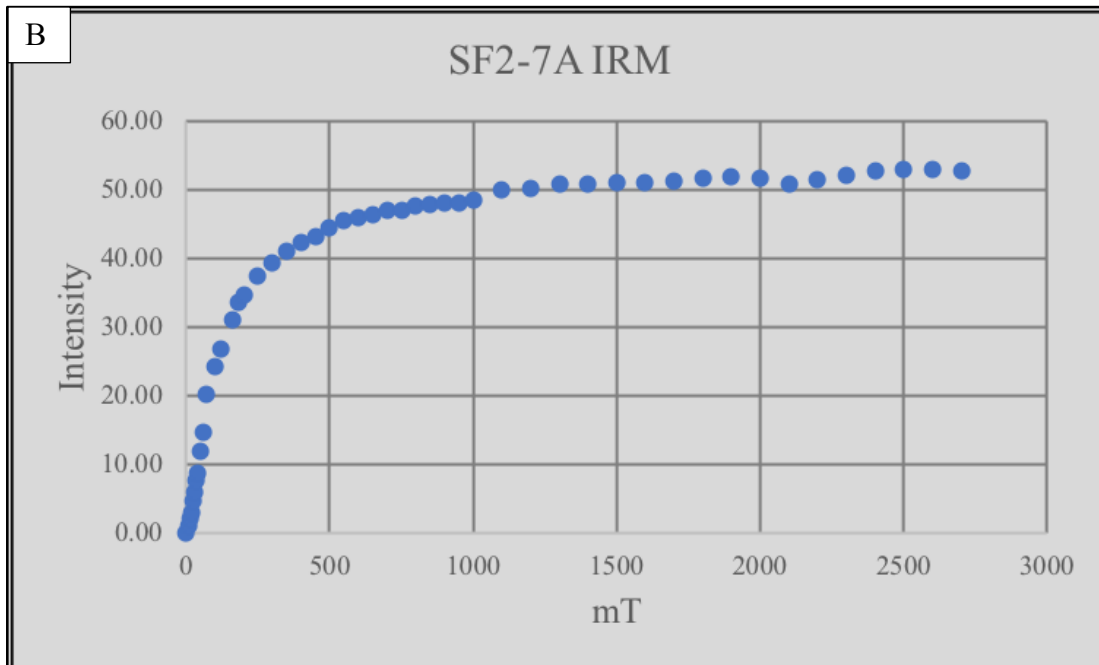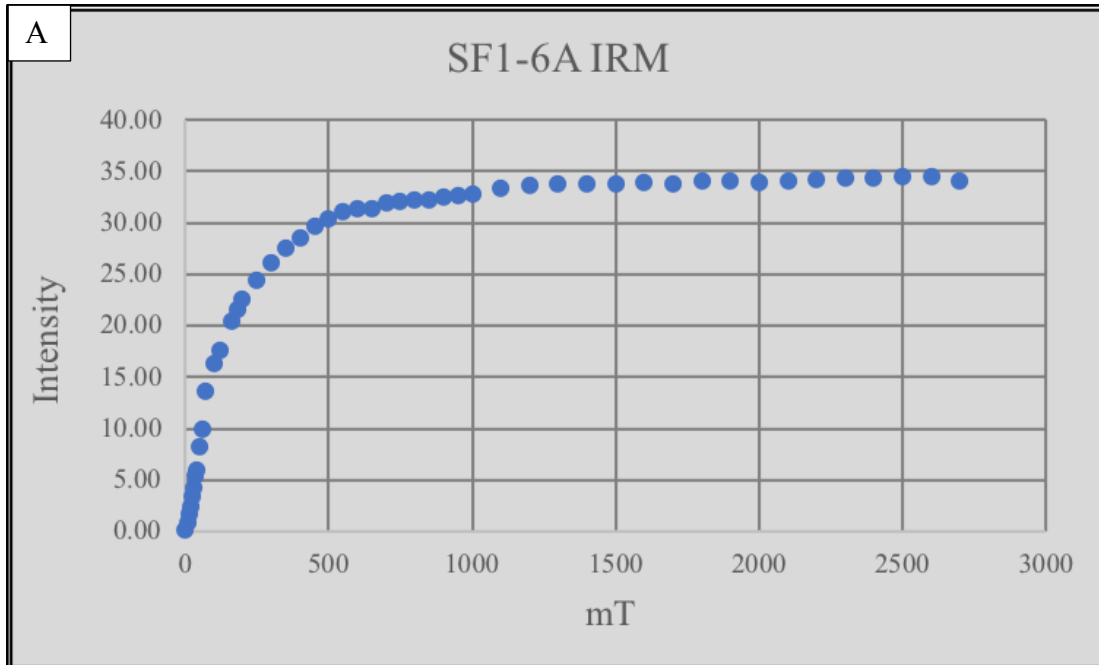
Figure 17: Graphs for two specimens illustrating IRM intensity versus mT.

5.3 Diagenesis and Paragenesis

Diagenetic and petrographic work can help place a relative time constraint on the hydrothermal activity which took place in the Womble Shale and can contribute to understanding the timing of remagnetization within the Shale. Petrographic work reveled a heavily veined calcareous sandstone in all thin sections. The petrographic results, confirmed by XRD analysis (Chung, 2003), illustrate that quartz and calcite are the dominant minerals in the veins, with the matrix composed of quartz, calcite, albite, dolomite, muscovite, clays, and peloids (Figure 18a, b). Stylolites are abundant (Figure 18b). Blocky, fractured quartz and twinned calcite occur in most veins (Figure 18c). Both detrital and authigenic (Figure 18d) quartz are located in the matrix. Several veins have calcite on the margin and blocky quartz in the center – indicating multiple fluid events beginning with calcite followed by quartz precipitation (Figure 18e).
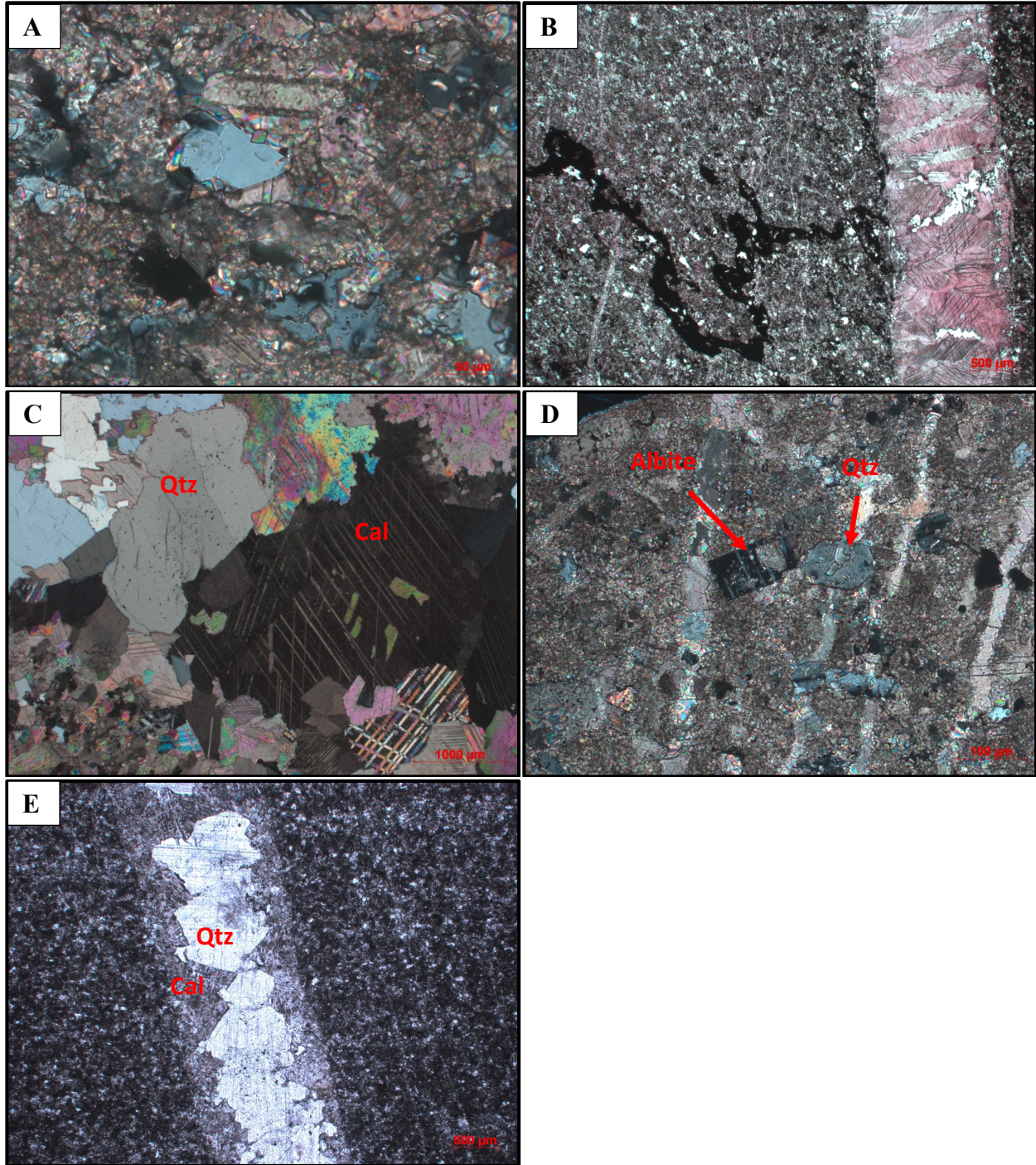
Figure 18: Photomicrographs of the Womble Shale including the matrix, veining, and stylolites. a) Matrix including quartz, calcite, albite, dolomite, and muscovite (XPL). b) Matrix and vein with a stylolite that extends from the matrix and one branch appears to follow the left side of the vein; stained with alizarin red (PPL). c) Large vein composed of twinned calcite and fractured quartz (XPL). d) Authigenic grains of albite and hexagonal quartz located in the matrix with calcite veins present (XPL). e) Vein with calcite on the edge of the vein and blocky quartz on the interior (PPL).

39

Veins with quartz and calcite are offset by stylolites (Figure 19a) and some veins contain stylolites internally (Figure 19b). However, some veins are not offset by stylolites (Figure 19c). Authigenic muscovite (Figure 19d) and quartz (Figure 19e) are present in some stylolites. The quartz within the stylolite in Figure 19e does not appear to be as fractured as the quartz located in most veins.

Within the matrix, dark grains, composed of illite and hematite, based on energy dispersive x-ray spectroscopy (EDS) analysis, are present. They have a dark reddish color from hematite staining (Figure 20a). Some are cubic and could be replaced pyrite whereas others could be replaced peloids. The grains are concentrated near the veins (Figure 20b) and are less abundant away from the veins (Figure 20c, d). This pattern suggests that the fractures around the veins were conduits for fluids that precipitated the clays and hematite.

Figures 21a and 21b show fibrous bands of muscovite and illite containing hematite. Hematite occurs within the clay bands in SEM (Figure 21c) based on EDS analysis. Illite, chlorite, and other clays have been identified in other studies within the Womble Shale (Weaber, 1958). Hydrocarbons, identified by carbon using the EDS analysis, are also present as seen in Figures 21c and 23d. Hematite is present replacing pyrite framboids (Figures 21c and d).

Detrital zircon and early diagenetic framboidal pyrite (Figure 22a) are present in the matrix. Likely hydrothermal minerals include sphalerite, barite, and authigenic apatite which are present throughout the matrix and in veins. Figure 22b shows the matrix with authigenic minerals including quartz, calcite, apatite, pyrite, as well as hydrocarbons. Authigenic anatase is also observed with a pyrite framboid in a quartz and calcite matrix (Figure 22c). Sphalerite (Figure 22d) and barite (Figure 22e) are also present in the matrix although it is difficult to

determine their paragenesis because cross cutting textural relationships are not clear. They probably represent different mineralizing events.
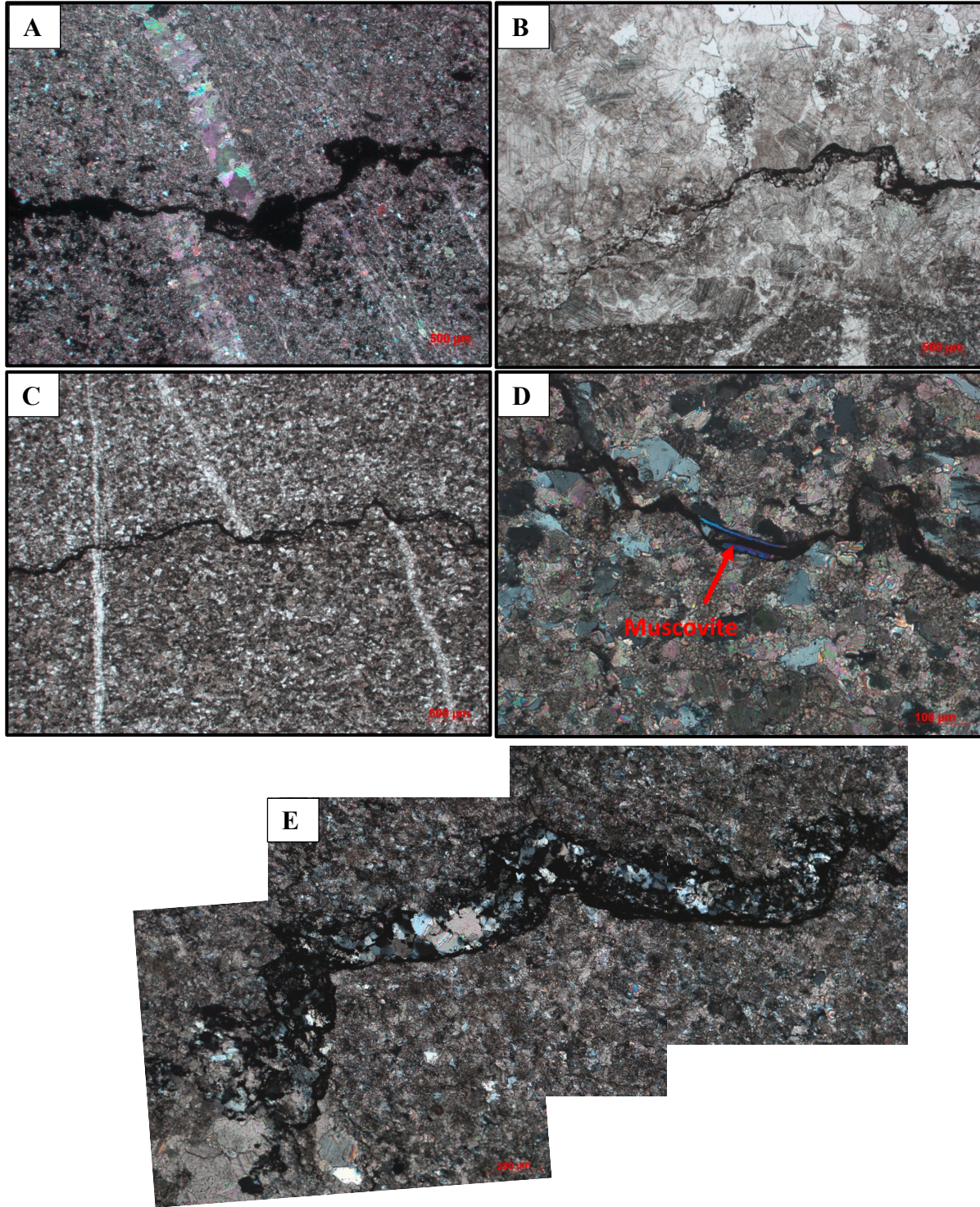
Figure 19: Photomicrographs of stylolites within the calcareous sandstone matrix and veins. a) Quartz and calcite vein offset my stylolite (XPL). b) Stylolite within large quartz and calcite vein (XPL). c) Two veins cross-cutting a stylolite – vein on the left is intact while the vein on the right is offset by a stylolite (PPL). d) Stylolite in matrix containing authigenic muscovite (XPL). e) Stylolite containing authigenic quartz (less fractured than quartz in veins) (XPL).
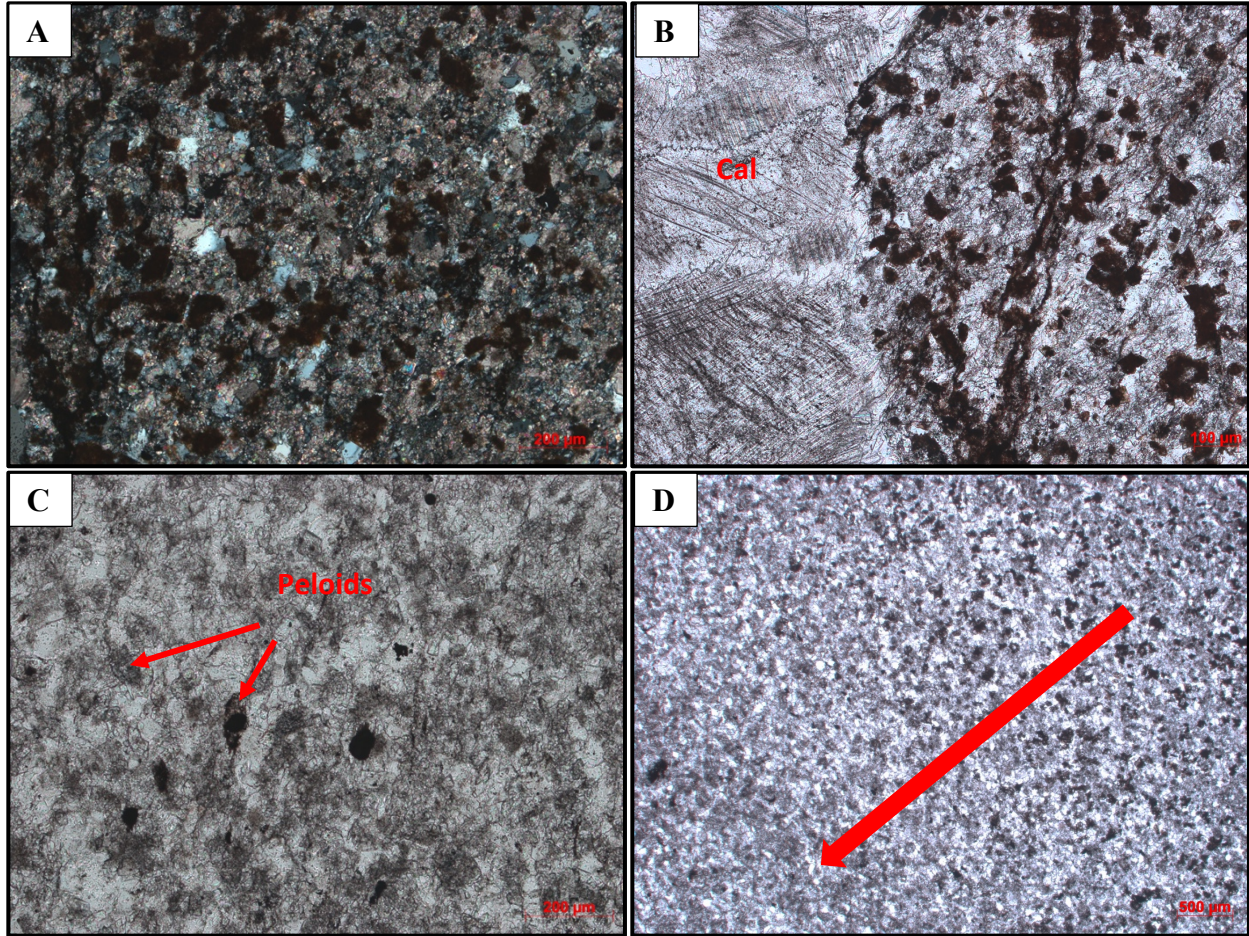
Figure 20: Photomicrographs of clays in calcareous sandstone matrix and in proximity to several veins. a) Matrix of the calcareous sandstone containing clays including hematite in close proximity to a vein (XPL). b) Clays adjacent to calcite vein in the matrix (PPL). d) Matrix of the calcareous sandstone containing less clays farther away from the vein than 22a and 22b and presence of peloids (PPL). d) Arrow represents direction moving away from the vein and a decrease in clay presence (PPL).
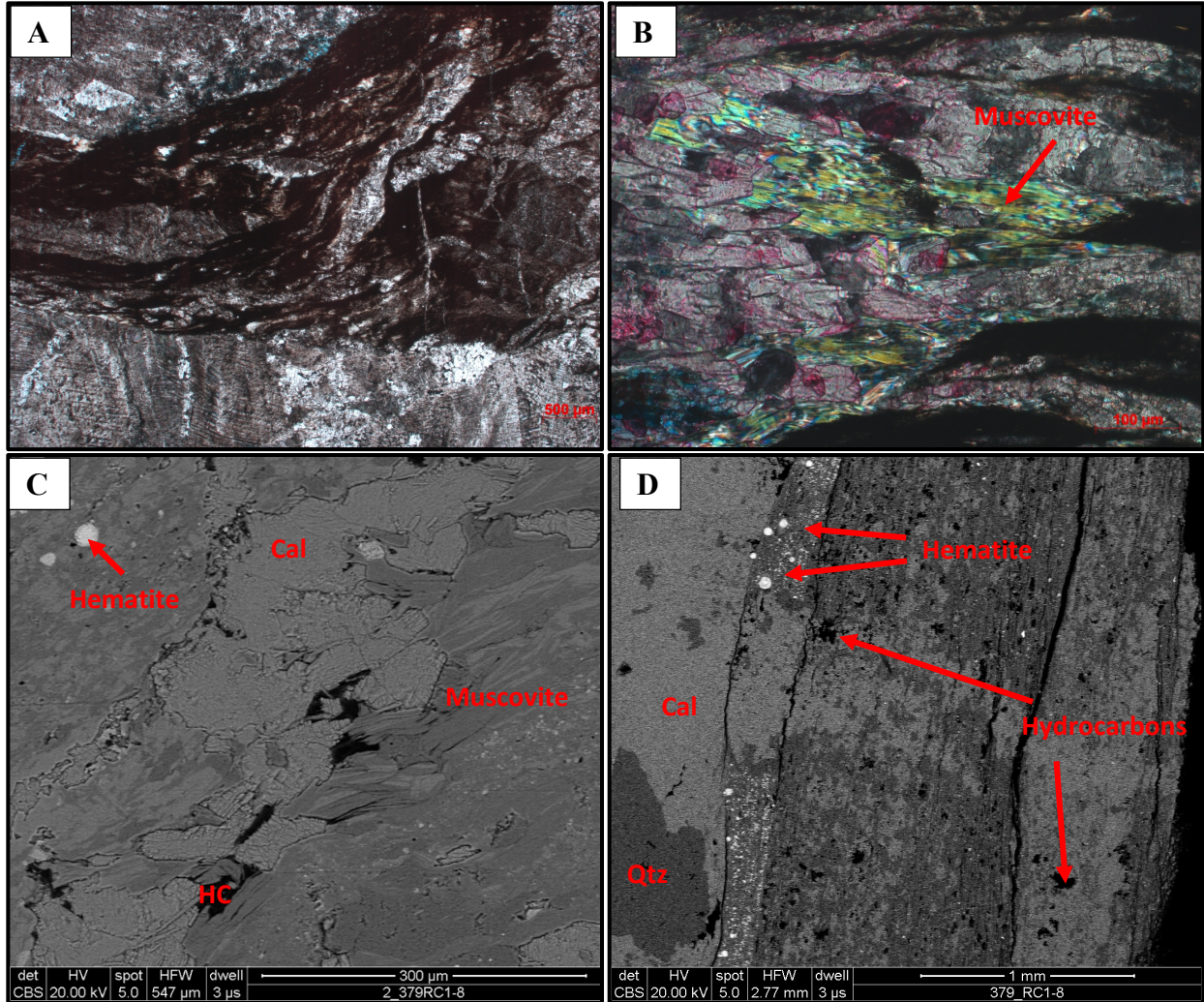
Figure 21: Clays within the calcareous sandstone matrix. a) Clay laminae containing hematite and muscovite (PPL). b) Muscovite within fibrous bands and alizarin red staining (XPL). c) Muscovite, hematite, and hydrocarbons in fibrous bands. d) Fibrous bands including muscovite and hematite with a calcite vein cutting through.
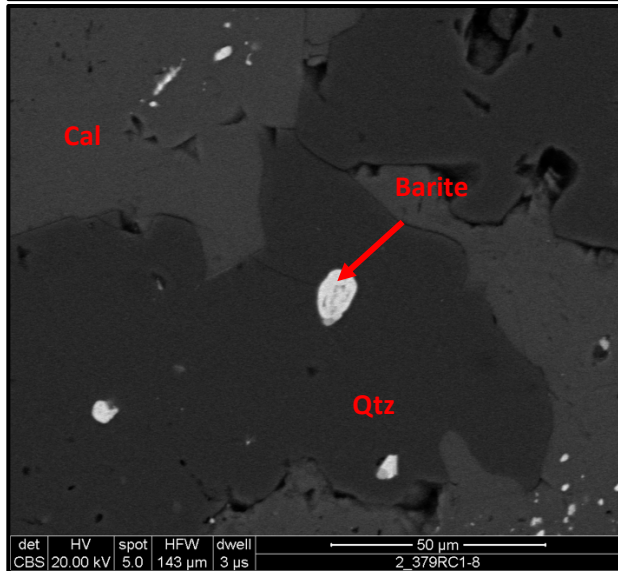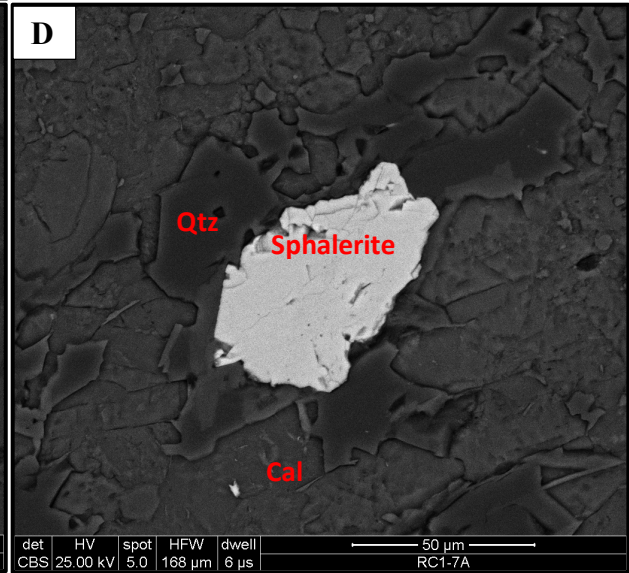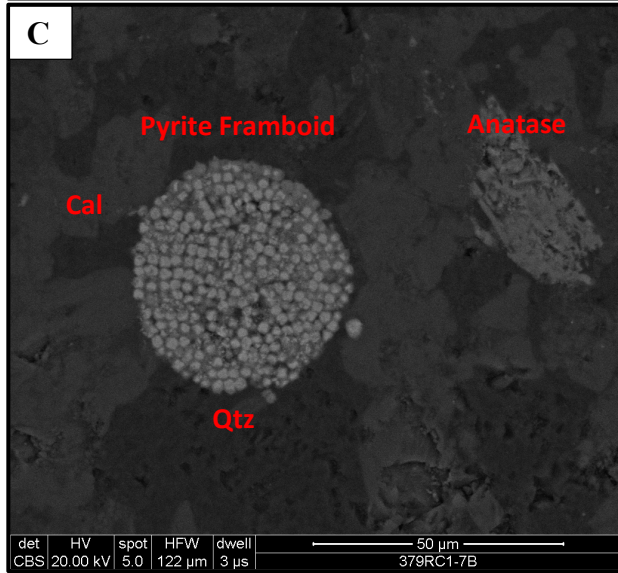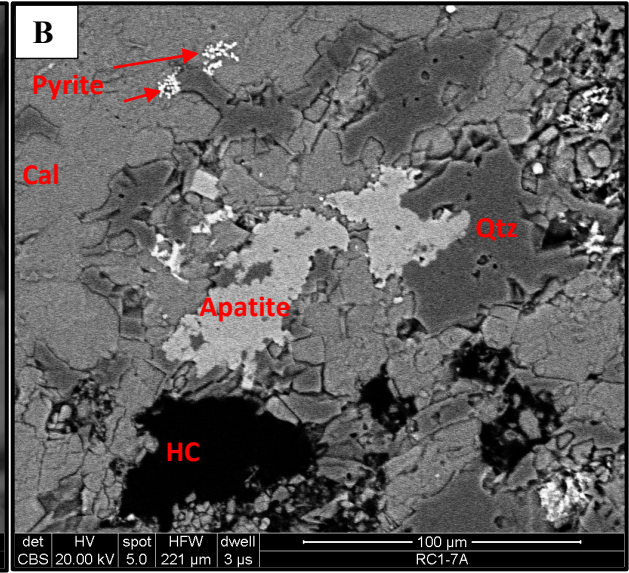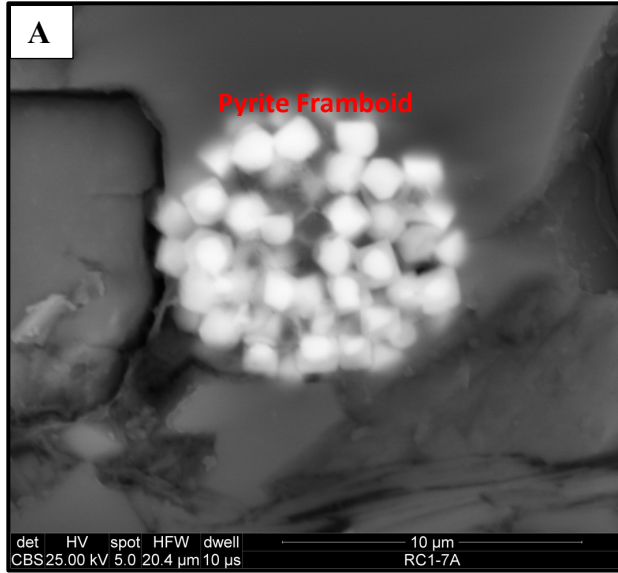
Figure 22: Energy dispersive x-ray spectroscopy (EDS) was used to identify minerals in SEM photos. a) Framboidal pyrite partly replaced by gray iron oxide, either hematite or magnetite. b) Calcareous sandstone matrix including quartz, calcite, apatite, hydrocarbons and pyrite. c) Pyrite framboid and authigenic anatase. d) Sphalerite in quartz and calcite. e) Barite located within quartz and calcite vein.

Rare earth element phosphate minerals monazite ($CePO_4$; Figure 23a and 23b) and xenotime (YPO_4; Figure 24a and b) are present and commonly found near quartz. A xenoblastic texture was identified in monazite grains (Figure 23) indicating detrital monazite is partially or completely dissolved – precipitation of new metamorphic monazite can take place on old grains (Rasmussen, 2007). Xenotime was identified using EDS by elevated levels of yttrium and phosphate (Figure 24b). Strontianite ($SrCO_3$ Figure 25a) was identified using EDS (Figure 25b) by the presence of strontium and oxygen – the calcium present in the EDS is being picked up by the surrounding calcite (Figure 25b).

Xenotime, monazite, and apatite are all reported to precipitate or dissolve depending on the changes in phosphate levels within a system (Spear and Pyle, 2002). Xenotime and monazite have been used in previous studies as geochronometers and geotemperatures to provide insight to diagenetic and hydrothermal changes (Gysi and Harlov., 2021). Xenotime is often linked to relatively low temperature hydrothermal activity and has been reported to form at temperatures between 100-120ºC within hydrothermal veins (Gysi and Harlov, 2021; Cook et al., 2013). Xenotime can form by several different processes – a diagenetically late overgrowth on detrital zircon, a low-grade metamorphic mineral, or can be produced by hydrothermal mineralization (McNaughton and Rasmussen, 2018; England et al., 2002). Xenotime in the Womble Shale is presumed to have formed by hydrothermal mineralization as is it observed within the quartz and calcite veins.

Monazite, commonly occurring with xenotime, can also form in a variety of ways – the most common occurrences include precipitation from a metamorphic hydrothermal fluid and magmatic monazite (Richter et al., 2018; Qui et al., 2020). Hydrothermal monazite is typically observed to contain lower thorium levels while magmatic monazite contains elevated thorium

levels (Qui et al., 2020). Hydrothermal monazite is also reported to sometimes have a xenoblastic texture which is observed in Figure 23 (Rasmussen and Muhling, 2007). Monazite in the Womble Shale is interpreted to be hydrothermal due to low thorium levels and a xenoblastic texture. Detrital monazite can become unstable in greenschist facies leading to partial or complete dissolution; monazite can then reprecipitate on old grains (Rasmussen and Muhling, 2007).
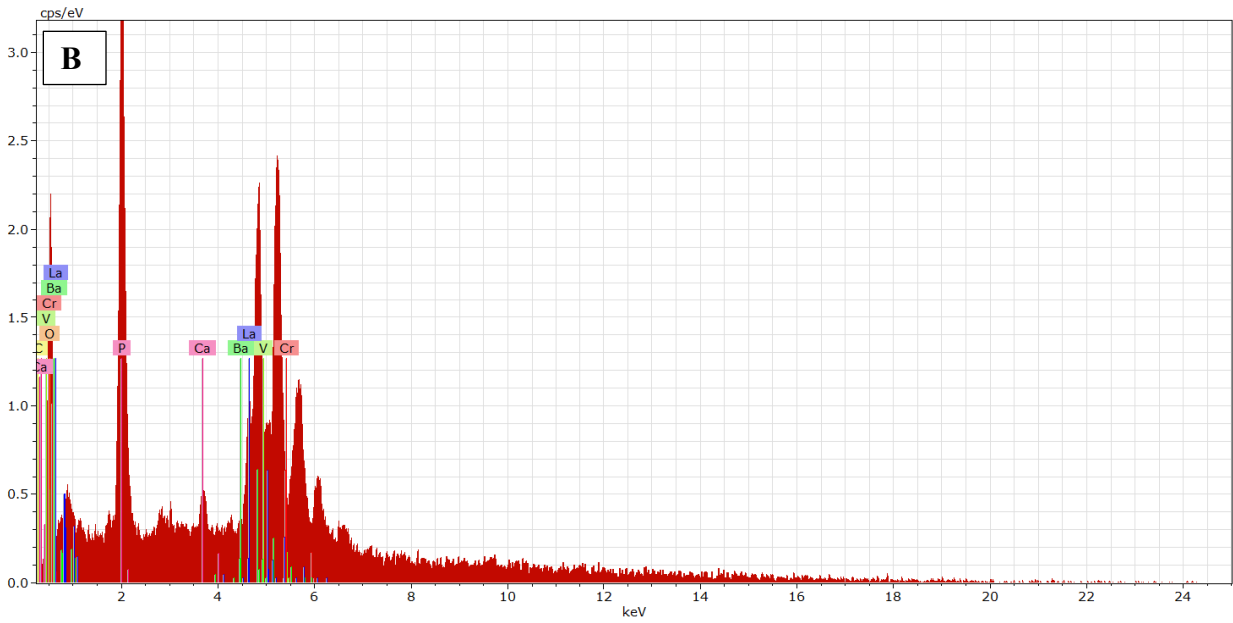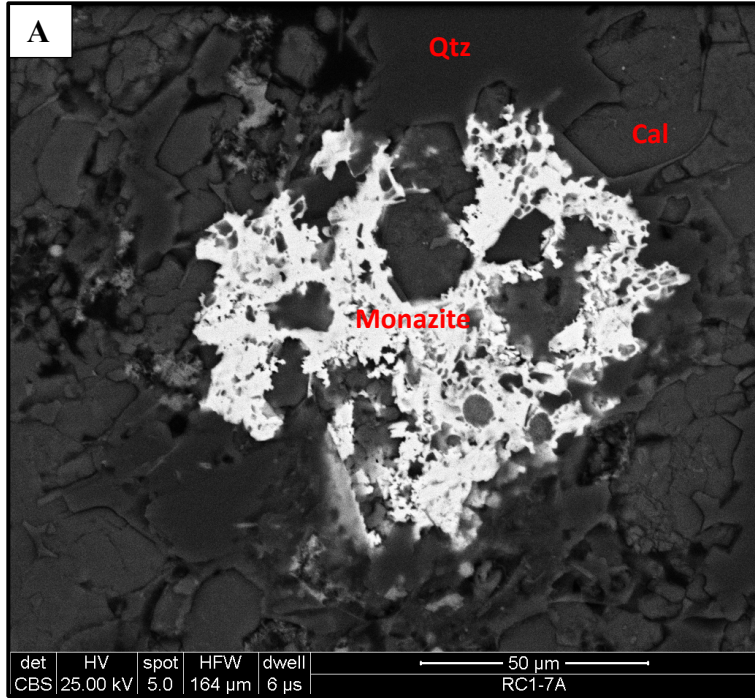
Figure 23: A) Monazite grain surrounded by quartz and calcite. B) EDS analysis of monazite.
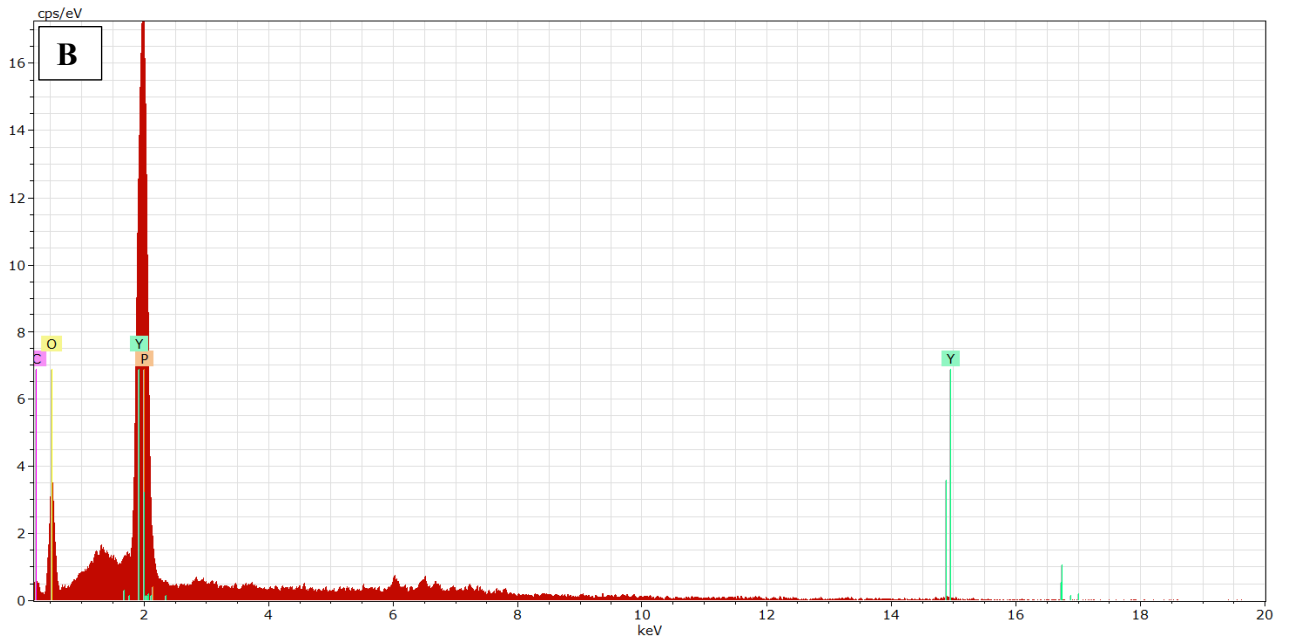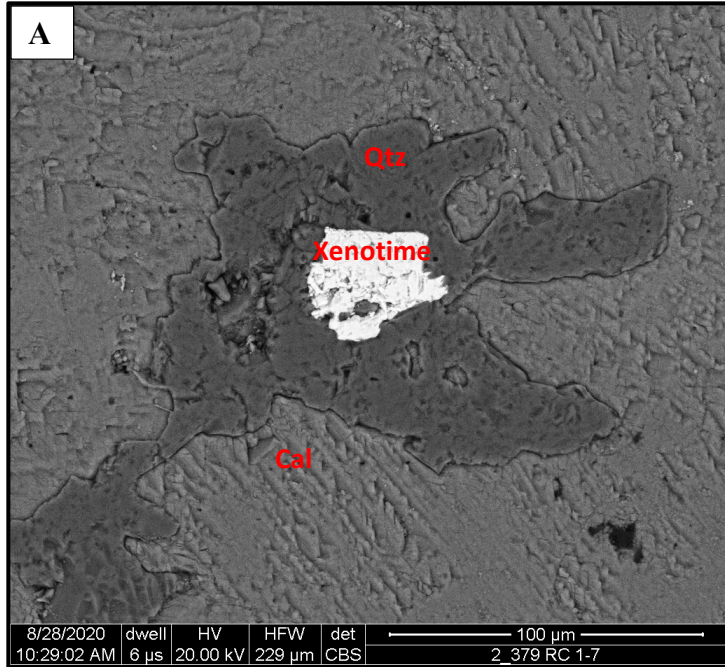
Figure 24: A) Xenotime located in quartz and calcite. B) EDS analysis of xenotime.
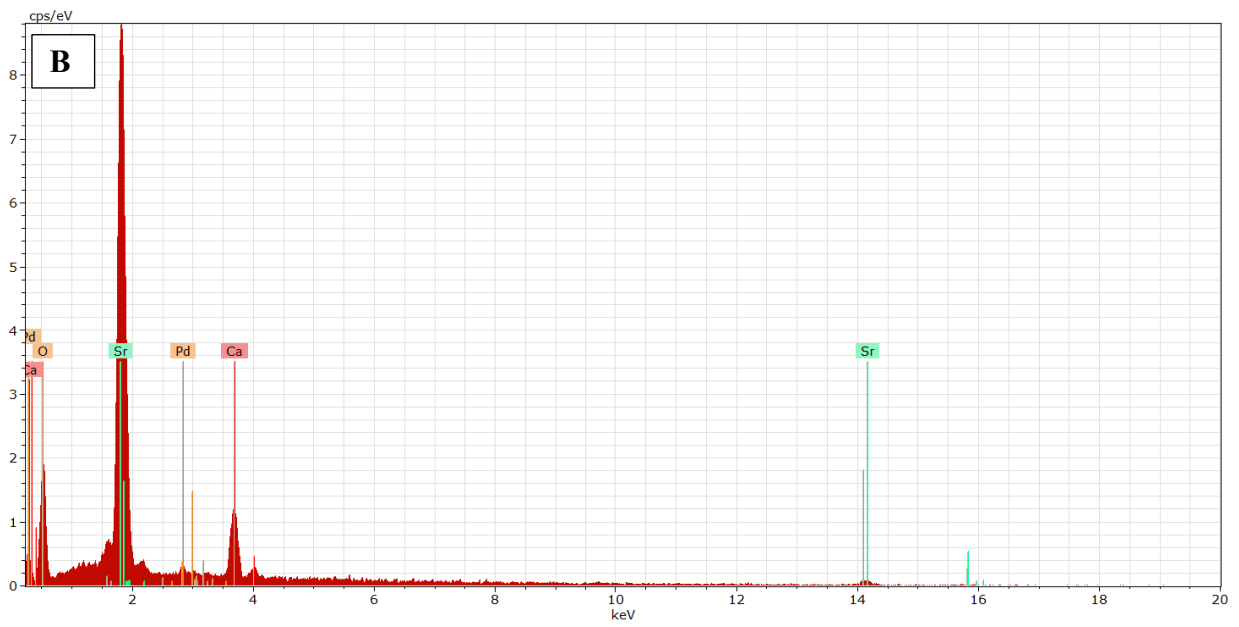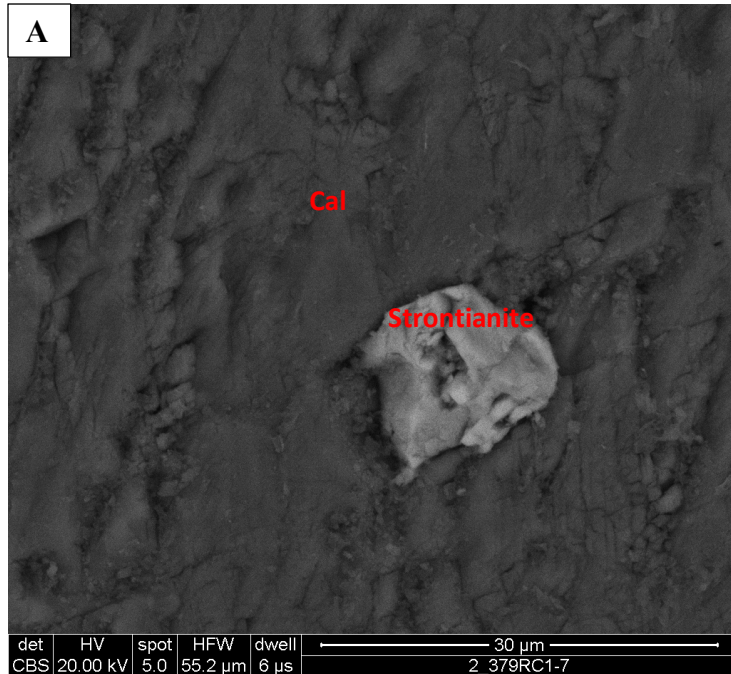
Figure 25: A) Strontianite located in calcite. B) EDS analysis of strontianite.

The paragenetic sequence (Figure 26) illustrates the outlined phases in relation to one another. Framboidal pyrite was early. The relative timing of the authigenic phases in the matrix are hard to determine because there are not cut by other features (e.g., veins). Many of these phases are interpreted to be hydrothermal in origin (sphalerite, xenotime, and monazite) and some are interpreted to be formed at the same time as the veins. The veins filled with calcite and quartz are interpreted to be late and syntectonic. This is consistent with Chung (2003) who investigated the veins and based on their orientations interpreted them to be syntectonic, forming during regional thrust fault events. The illite and muscovite clays are also interpreted to be late. The pattern around some veins suggests that fluids emanating from the fractures caused the precipitation of the clays and hematite.

It is also likely that the veins within the calcareous sandstone units of the Womble Shale formed before factures in the shale units of the Womble Shale (Chung, 2003). Chung (2003) provides several explanations for this: the shale fracture directions do not align with transport directions, increased clay content in shales prevented fracturing until uplift (and after calcareous sandstone fracturing), and the calcareous sandstone beds served as the source rock for vein materials so calcareous sandstone fractures were filled first due to proximity. Most of the stylolites are interpreted to be syntectonic as is the twinning of the calcite and fracturing of quartz. The hydrocarbons are interpreted to be late and have been reported to be biodegraded and contain organic matter which is most likely type II kerogen by Fowler and Douglas (1984). Low-grade metamorphism, orogenic deformation, multiple hydrothermal fluids events, and uplift of the Womble Shale all contributed to the diagenesis of the unit.

Events	Early ⟶ Late		
Matrix			
Detrital Quartz			
Detrital Zircon			
Calcite			
Framboidal Pyrite			
Dolomite			
Sphalerite			
Apatite			
Barite			
Xenotime			
Monazite			
Strontianite			
Anatase			
Authigenic Albite			
Authigenic Quartz			
Hematite			
Muscovite/illite clays			
Hydrocarbons			
Veins			
Calcite			
Quartz			
Stylolite offset veins			
Stylolite			
Zircon			
Monazite			
Muscovite			

Figure 26: Paragenetic sequence of events and phases identified with the Womble Shale calcareous sandstone.

53

6. Discussion

The magnetic component removed by AF treatment and the unblocking temperatures below 580ºC, suggest this component resides magnetite (Figures 10, 11). The IRM acquisition results are consistent with this interpretation magnetization which confirmed the presence of both a lower and higher coercivity minerals. The AF results and the significant decay below 325ºC are consistent with pyrrhotite but the decay to 400ºC suggests magnetite. Demagnetization did not reveal different pyrrhotite (<325ºC) and magnetite (325-400ºC) components. As described below, significant magnetic intensity remained after the AF treatment, which suggests that a high coercivity mineral such as hematite remains to be demagnetized. Because only one component was revealed during AF treatment, it is interpreted to reside in magnetite.

Based on slightly different dips, the best grouping of the directions (southeasterly declination and moderate positive inclinations) suggest it is post tilting magnetization. The pole of this magnetization is apparently late Mississippian but because of the possibility of contamination, the age should be viewed with caution. Because unblocking temperatures are low (400ºC) and relatively high burial temperatures (~300ºC), this component is likely a thermoviscous remnant magnetization (TVRM). The origin of the magnetite that carries this TVRM is unknown.

The removal of the southeasterly and shallow component during thermal demagnetization after AF treatment suggests that it resides in hematite. It is removed at relatively low temperatures (<400ºC) which probably indicates fine grained hematite (Swanson-Hysell et al., 2019). The previous AF treatment removed the magnetite component. The hematite component is interpreted as a post tilting ChRM with southeasterly declinations and shallow inclinations. It was not possible to collect samples for fold test because appropriate outcrops could not be found.

Location of such outcrops should be an objective of future work. The low maximum unblocking temperatures (400°C) and a maximum burial temperature of 300°C interpreted from chlorite crystallinity (Johnson et al., 2019) and through conodont color alteration indices by Shelton et al. (1986), suggests the ChRM could be a TVRM (e.g., Dunlop & O¨zdemir, 1997) or a thermochemical remnant magnetization influenced by the moderate temperatures. The magnetite component is probably older than the hematite component and is interpreted as a TVRM that formed during cooling from elevated burial temperatures. It is unlikely that there could be two TVRMs of different ages in the rock. This assumes that the magnetite component is older that the hematite component, and that the contamination is not the reason for the age difference. The younger hematite component is interpreted as a thermochemical remnant magnetization. This hematite component is interpreted to date one episode of hydrothermal alteration in the Womble shale.

Although the age of hydrothermal activity within the Ouachita Mountains is poorly constrained, three studies have placed estimated timing on the formation of the veining. Rb-Sr and K-Ar was used to date adularia by Bass and Ferrara (1969) which dated the veins at 287-279 Ma (Rb-Sr) and 214-190 Ma (K-Ar). Shelton et al., (1986) used K-Ar to date adularia and constrained the age of the veins to 262± Ma. Piper (2011) used quartz-calcite isotope thermometry, vitrinite reflectance temperatures, and fluid inclusion data to identify temperature and pressure conditions of the veins. Using the constrained pressure, depth of formation of the veins was identified and plotted on a burial curve which showed early to middle Pennsylvanian formation of veins (Piper, 2011). If a thermochemical remnant magnetization is present, remagnetization timing closely resembles the vein age that Piper (2011) obtained.

The relationship between the rock matrix, veins, and stylolites can provide insight to the timing of diagenetic-hydrothermal activity and deformation within the Womble Shale. Stylolites within the Womble Shale are generally parallel to bedding, but several stylolites which are perpendicular to bedding were identified. Figure 18b shows a stylolite next to a vein and following the vein boundary indicating that the vein formation proceeded the stylolite. Many veins are also offset by stylolites as shown in Figure 19a, further indicating that some veins formed before the stylolites. Stylolites are also observed within veins, as seen in Figure 19b, which also supports the previously stated order of occurrence. However, it does not appear that all veins occurred before stylolites as some veins are not offset by the same stylolite as seen in Figure 19c. Evidence of deformation occurs in both the matrix and veins of the Womble Shale primarily in the form of stylolites, twinned calcite, and fractured quartz. Because evidence of deformation appears to occur both before and after formation of quartz and calcite veins and is even present within some veins, the quartz and calcite veins are interpreted as syntectonic.

Several major alteration events occurred after formation of the Womble Shale: hydrothermal activity which produced quartz and calcite veins during multiple fluid events, precipitation of authigenic minerals present in the matrix, greenschist burial metamorphism, and deformation during the Ouachita orogeny which produced physical evidence of deformation such as stylolites, twinned calcite, and blocky quartz (Figure 25). These events could have occurred concurrently.

Positive quartz-calcite isotopic fractionation values from Piper (2011) and Richard et al. (2002) indicate that precipitation of quartz and calcite occurred simultaneously and from the same fluid. The fractionation values also help to determine that quartz and calcite crystallized simultaneously to form the veins (Zheng, 1993). A study by Kirschner et al. (1995) on quartz and

calcite veins in a greenschist facies of the Swiss Alps reports that the structural texture of fibrous

quartz and calcite minerals within veins are banded together which would have had to precipitate

simultaneously (Durney, 1972; Durney and Ramsey, 1973). As previously stated, fibrous calcite

was reported in the Womble Shale by Chung (2003) and Cervantes and Wiltschko (2010).

Although the age of the veins is still an open question, the origination of vein fluid is

better documented. A comparison of oxygen isotope data of veins versus their host rock by

Richards et al. (2002) identifies that the host rock minerology has significant influence of vein

formation. A combination of advection and diffusion processes formed the veins within the

Ouachitas – seismic or dilational pumping moved fluids by advection which helped vein material

to diffuse from the host rock and transfer to fractures (Richards et al. 2002; Gray et al. 1991;

Fisher and Brantley, 1992). Calcite-rich beds in the calcareous sandstone are interpreted to be the

source of the vein material (Chung, 2003); Richards et al. (2002) also identifies that veins which

contain predominantly calcite are only located in calcite-rich host rocks. The migration fluids by

advection occurs on a 10 -100 meter scale (Richards et al. 2002). Another study by Etheridge

(1983) proposed that quartz dissolution and precipitation can create convective recirculation of

fluids. Quartz dissolves at higher temperatures, migrates upwards, and precipitates at lower

temperatures creating continuous precipitation of minerals in veins (Etheridge, 1983).

Circulation by this process would be blocked by impermeable units within the section which

would suggests it would not take as take place on a large scale (Richards et al., 2002; Wood and

Walther, 1986). Chung (2003) states that the veins within calcareous sandstone layers are

parallel to the estimated N-S average tectonic stress direction. Both diffusion and advection

contribute to the fluid flow and accumulation of vein material in fractures during which

precipitation and crystallization occurred simultaneously in one event while deformation was occurring (Piper, 2011; Richards et al., 2002; Chung, 2003).

Several other studies conducted on units within proximity to the Womble Shale outcrop suggest that post orogenic fluid flow events occurred during the Late Paleozoic after collision and deformation (Shelton et al., 1986; Elmore et al., 1993; Roberts, 2017). As previously stated, Shelton et al., (1986) identified post-collisional hydrothermal alteration in the Ouachitas which extended into the Permian based on adularia dating. Elmore et al. (1993) identified a Permian-aged CRM residing in hematite in the Viola Formation in the Arbuckle Mountains which originated from basinal fluids – indicating that fluid mineralization occurred during the late Permian. In the Woodford Shale, Roberts (2017) identified a Late Permian CRM or TCRM within magnetite associated with hydrothermal minerals indicating that a Late Permian fluid event occurred. In contrast, in a study in the Bigfork Chert within the western Ouachita Mountains, Hillegeist et al. (1992) reported a syndeformational CRM. The timing is consistent with the Late Mississippian to Late Pennsylvanian syntectonic magnetization found in the Womble Shale.

7. Conclusions

The Womble Shale has been diagenetically altered by extensive hydrothermal alteration, and deformation within the Ouachita Mountains. Physical evidence of deformation such as stylolites are observed to have formed before and after quartz and calcite veins. Deformation is also identified based on twinned calcite and fractured quartz in the veins. Hydrothermal minerals such as xenotime, monazite, biotite, and sphalerite are present in the matrix and in veins. They probably formed in several episodes. Other authigenic phases are also observed in the matrix such as authigenic quartz and albite.

The AMS fabric in the Womble Shale is complex and is interpreted to be influenced by burial, tectonic, and diagenetic fabrics. A post titling TVRM is held in magnetite and is interpreted to be contaminated by a modern VRM because of curved demagnetization paths. A Late Pennsylvanian thermochemical remnant magnetization which resides in hematite and is interpreted as post tilting, is also present. This component is interpreted to have been caused by the hydrothermal alteration which precipitated hematite. Hydrothermal alteration and deformation are interpreted to have occurred simultaneously within the Womble Shale. This contrasts with other studies which report post orogenic hydrothermal activity in the Ouachitas (e.g., Shelton et al., 1986; Elmore et al., 1993; Roberts, 2017).

References

Arbenz, J. K., 1984. A structural cross section through the Ouachita Mountains of western Arkansas. In: Stone, C. G., Haley, B. R., (Eds), A guidebook to the geology of the central and southern Ouachita Mountains, Arkansas, Little Rock, Arkansas Geological Commission Miscellaneous Publication, pp. 76-85.

Bass, M.N., Ferrara, G., 1969. Age of adularia and metamorphism, Ouachita Mountains, Arkansas. American Journal of Science 267, 491-498.

Blythe, A. E., Sugar, A., Phipps, S. P., 1988. Structural profiles of Ouachita Mountains, western Arkansas. American Association of Petroleum Geologists Bulletin 72, 810-819.

Buthman, D. B., 1985. Stratigraphy and Structural Style of the Mazarn, Blakely and Womble Formations in the Ouachita Core Near Norman, Arkansas.

Cervantes, P., Wiltschko, D. V., 2010. Tip to midpoint observations on syntectonic veins, Ouachita orogen, Arkansas: Trading space for time. Journal of Structural Geology, 32(8), 1085-1100.

Chung, J. W., 2003 "The investigation on fibrous veins and their host from Mt. Ida, Ouachita Mountains, Arkansas." [Thesis, Texas A&M University]. Texas A&M University Libraries.

Cook, N.J., Ciobanu, C.L., O'Rielly, D., Wilson, R., Das, K., Wade, B., 2013. Mineral chemistry of rare earth element (REE) mineralization, Browns Ranges, Western Australia. Lithos 172-173, 192–213.

Curiale, J. A., Harrison, W. E., and Smith, G., 1983. Sterane distribution of solid bitumen pyrolyzates. Changes with biodegradation of crude oil in the Ouachita Mountains, Oklahoma. Geochimica et Cosmochimica Acta, 47(3), 517-523.

Dunlop, D. J., O¨zdemir, O¨., 1997. Rock Magnetism: Fundamentals and Frontiers. Cambridge Univ. Press, New York, 573 pp.

Dunlop, D. J.,, Argyle, K. S., 1991. Separating multidomain and single-domain-like remanences in pseudo-single-domain magnetites (215–540 nm) by low-temperature demagnetization. Journal of Geophysical Research: Solid Earth, 96(B2), 2007-2017.

Durney, D. W., 1972, Deformation history of the western Helvetic nappes, Valais, Switzerland [Ph.D. thesis]: London, University of London, 327 p.

Durney, D. W., Ramsay, J. G., 1973. Incremental strain measured by syntectonic crystal growths, in de Jong, K., and Scholten, R., eds., Gravity and tectonics: New York, John Wiley, p. 67–96.

Elmore, R. D., London, D., Bagley, D., Fruit, D., & Gao, G., 1993. Remagnetization by basinal fluids: testing the hypothesis in the Viola Limestone, southern Oklahoma. Journal of Geophysical Research: Solid Earth, 98(B4), 6237-6254.

England, G.L., Rasmussen, B., McNaughton, N.J., Fletcher, I.R., Groves, D.I., Krapez, B., 2002. SHRIMP U− Pb ages of diagenetic and hydrothermal xenotime from the Archaean Witwatersrand Supergroup of South Africa. Terra Nova 13, 360–367.

Etheridge, M. A., 1983. Differential stress magnitudes during regional deformation and metamorphism: upper bound imposed by tensile fracturing. Geology, 11(4), 231-234.

Fisher, R., 1953. Dispersion on a Sphere. Proceedings of the Royal Society of London. Series A, Mathematical and Physical Sciences (1934-1990), 217(1130), 295-305.

Fisher, D.M., and Brantley, S.L., 1992. Models of quartz overgrowth and vein formation: Deformation and ep- isodic fluid flow in an ancient subduction zone: Journal of Geophysical Research, v. 97, p. 20,043–20,061.

Fowler, M. G., Douglas, A. G., 1984. "Distribution and structure of hydrocarbons in four organic-rich Ordovician rocks." Organic Geochemistry Volume 6 pp.105-114 DOI: 10.1016/0146-6380(84)90031-7.

Gleason, J. D., Finney, S. C., & Gehrels, G. E., 2002. Paleotectonic implications of a Mid-to Late-Ordovician provenance shift, as recorded in sedimentary strata of the Ouachita and southern Appalachian mountains. The Journal of geology, 110(3), 291-304.

Gleason, J. D.; Patchett, P. J.; Dickinson, W. R.; and Ruiz, J., 1994. Nd isotopes link Ouachita turbidites to Appalachian sources. Geology 22:347–350.

Glick, E. E., Stone, C. G., Howe, J. R., 1991. "Regional Environments of Deposition During Cambrian and Ordovician Time in Western Arkansas." Oklahoma Geological Survey Circular 92, 1991 pg. 217.

Gray, D.R., Gregory, R.T., and Durney, D.W., 1991, Rock- buffered fluid-rock interaction in deformed quartz-rich turbidite sequences, eastern Australia: Journal of Geo- physical Research, v. 96, p. 19,681–19,704.

Gysi, A. P., & Harlov, D., 2021. Hydrothermal solubility of TbPO4, HoPO4, TmPO4, and LuPO4 xenotime endmembers at pH of 2 and temperatures between 100 and 250° C. Chemical Geology, 567, 120072.

Haley, B. R., and Stone, C., 1976. CoGeo map of Arkansas: U.S. Geological Survey and Arkansas Geological Commission, scale 1:24,000.

Heslop, D., McIntosh, G. & Dekkers, M. J., 2004. Using time- and temperature- dependent Preisach models to investigate the limitations of modeling isothermal remanent magnetization acquisition curves with cumulative log Gaussian functions. Geophysical Journal International, **157**, 55–63.

Hillegeist, T. K., Fruit, D. J., Elmore, R. D., 1992. "Syndeformational magnetization in the Ordovician Bigfork Chert at Black Knob Ridge, western Ouachita Moutains, southern Oklahoma." Earth and Planetary Science Letters, 109.

Howard, J. M and Stone, C., 1988, Quartz crystal deposits of the Ouachita Mountains, Arkansas and Oklahoma. Arkansas Geological Commission Miscellaneous Publication, pp. 63-71.

Johnson, H. E., Wiltschko, D. V., & Harris, J. P., 2019. Diagenetic to incipient metamorphic zones of the Benton Uplift, Ouachita Orogen, Arkansas, USA. *GSA Bulletin*, *132*(5-6), 977-986.

Johnson, K. S., 1996 "Geology of Oklahoma." Oklahoma Geology Survey Special Publication pages 1-9.

Kirschvink, J. L. (1980). The least-squares line and plane and the analysis of palaeomagnetic data. Geophysical Journal International, 62(3), 699–718. https://doi.org/10.1111/j.1365-246X.1980.tb02601.x

Kirschner, D. L., Sharp, Z. D., Masson, H., 1995. Oxygen isotope thermometry of quartz- calcite veins; Unveiling the thermal-tectonic history of the subgreenschist facies Morcles nappe (Swiss Alps). Geological Society of American Bulletin 107, 1145- 1156.

Kruiver, P. K., Dekkers, M. J. & Heslop, D., 2001. Quantification of magnetic coercivity components by the analysis of acquisition curves of isothermal remanent magnetization. Earth and Planetary Science Letters, **189**, 269–276.

Lowe, D. R., 1985. Ouachita trough: Part of a Cambrian failed rift system. Geology, 13(11), 790-793.

Lowrie, W., 1990. Identification of ferromagnetic minerals in a rock by coercivity an unblocking temperature properties, Geophys. Res. Lett., 17, 159–162, doi:10.1029/GL017i002p00159.

McCabe, C., R. Van der Voo, and M.M. Ballard, 1984, Late Paleozoic remagnetization of the Trenton Limestone: Geophysical Research Letters, American Geophysical Union, **11**, 979-982, doi: 10.1029/GL011i010p00979

McFarland, J. D., 1998. Stratigraphic summary of Arkansas (Vol. 36). Little Rock: Arkansas Geological Commission.

McNaughton, N.J., Rasmussen, B., 2018. Geochemical characterisation of xenotime formation environments using U− Th. Chem. Geol. 484, 109–119.

Miser, H. D., & Purdue, A. H., 1929. Geology of the De Queen and Caddo Gap Quadrangles, Arkansas. US Government Printing Office.

Miser, H. D., 1959, Structure and vein quartz of the Ouachita Mountains of Oklahoma and Arkansas. In: The geology of the Ouachita Mountains, a symposium: Dallas and Ardmore Geological Societies, pp. 30-43.

Patchett, P. J.; Ross, G. M.; and Gleason, J. D., 1999. Continental drainage in North America during the phanerozoic from Nd isotopes. Science 283:671–673.

Piper, J. A., 2011 "The Thermal Evolution of the Ouachita Orogen, Arkansas and Oklahoma from Quartz-Calcite thermometry and Fluid Inclusion Thermobarometry." [Thesis, Texas A&M University]. Texas A&M University Libraries.

Qiu, K.F., Yu, H.C., Deng, J., McIntire, D., Gou, Z.Y., Geng, J.Z., Chang, Z.S., Zhu, R., Li, K.N. and Goldfarb, R., 2020. The giant Zaozigou Au-Sb deposit in West Qinling, China: magmatic-or metamorphic-hydrothermal origin?. *Mineralium Deposita*, *55*(2), pp.345-362.

Rasmussen, B., & Muhling, J. R., 2007. Monazite begets monazite: evidence for dissolution of detrital monazite and reprecipitation of syntectonic monazite during low-grade regional metamorphism. Contributions to Mineralogy and Petrology, 154(6), 675-689.

Richards, I., Connelly, J.B., Gregory, R.T., Gray, D.R., 2002. The importance of diffusion, advection, and host-rock lithology on vein formation a stable isotope study from the Paleozoic Ouachita orogenic belt, Arkansas and Oklahoma. Geological Society of America Bulletin 114, 1343-1355.

Richter, L., Diamond, L. W., Atanasova, P., Banks, D. A., & Gutzmer, J., 2018. Hydrothermal formation of heavy rare earth element (HREE)–xenotime deposits at 100° C in a sedimentary basin. Geology, 46(3), 263-266.

Roberts, J., 2017. A diagenetic and paleomagnetic study of the Woodford Shale, Oklahoma, USA.

Roberts, J., Heij, G., Elmore, R. D., 2019. Palaeomagnetic dating of hydrothermal alteration in the Woodford Shale, Oklahoma, USA. Geological Magazine, 156, 2043–2052. doi:10.1017/S0016756819000360.

Shelton, K. L., Reader, J. M., Ross, L. M., Viele, G. W., & Seidemann, D. E., 1986. Ba-rich adularia from the Ouachita Mountains, Arkansas; implications for a postcollisional hydrothermal system. *American Mineralogist*, *71*(7-8), 916-923.

Smith, D. L., Jenkins, D. T., 1984. Paleomagnetic Measurements in the Eastern Ouachita Mountains, Arkansas. Department of Geology, University of Florida.

Spear, F. S., & Pyle, J. M., 2002. Apatite, monazite, and xenotime in metamorphic rocks. Reviews in Mineralogy and Geochemistry, 48(1), 293-335.

Stone, C. G., & Sterling, P. J., 1962. New lithologic marker horizons in Ordovician rocks, eastern Ouachitas of Arkansas. AAPG Bulletin, 46(3), 387-390.

Stone, C. G., W. V. Bush., 1982. General geology and mineral resources of the Ouachita Mountains, Arkansas. Proceedings of the 22nd Forum on the Geology of Industrial Minerals pg. 87-106.

Suneson, N. H., 1995. The Geology of the Broken Bow Uplift: An Introduction and Field-Trip guide. Oklahoma Geologic Survey.

Sutton, S. J., & Land, L. S., 1996. Postdepositional chemical alteration of Ouachita shales. *Geological Society of America Bulletin*, *108*(8), 978-991.

Swanson-Hysell, N. L., Fairchild, L. M., and Slotznick, S. P. (2019). Primary and secondary red bed magnetization constrained by fluvial intraclasts. Journal of Geophysical Research: Solid Earth, 124. https://doi.org/10.1029/2018JB017067

Thomas, W. A., 1991. The Appalachian-Ouachita rifted margin of southeastern North America. Geol. Soc. Am. Bull. 103:415–431.

Torsvik, T.H., Van der Voo, R., Preeden, U., Mac Niocaill, C., Steinberger, B., Doubrovine, P.V., Van Hinsbergen, D.J., Domeier, M., Gaina, C., Tohver, E. and Meert, J.G., 2012. Phanerozoic polar wander, palaeogeography and dynamics. *Earth-Science Reviews*, *114*(3-4), pp.325-368.

Warnock, A.C., Kodama, K.P. and Zeitler, P.K., 2000. Using thermochronometry and low-temperature demagnetization to accurately date Precambrian paleomagnetic poles. *Journal of Geophysical Research: Solid Earth*, *105*(B8), pp.19435-19453.

Weaver, C. E., 1958. The effects and geologic significance of potassium "fixation" by expandable clay minerals derived from muscovite, biotite, chlorite, and volcanic material. American Mineralogist: Journal of Earth and Planetary Materials, 43(9-10), 839-861.

Wood, B.J., and Walther, J.V., 1986. Fluid flow during metamorphism and its implications for fluid-rock ra- tios, in Walther, J.V., and Wood, B.J., eds., Fluid-rock interactions during metamorphism: New York, Spring- er-Verlag, p. 91–108.

Zheng, Y., 1993. Calculation of oxygen isotope fractionation in anhydrous silicate minerals. Geochimica et Cosmochimica Acta 57, 1079-1091.

Zijderveld, J. D. A. 1967. The natural remanent magnetizations of the Exeter volcanic traps (Permian, Europe). Tectonophysics4, no. 2 (1967): 121-153.

Appendix 1: Paleomagnetic samples and subjected tests and thin section analysis

Sample Name	AMS	LTD	AF	Thermal
379RC1-5A	X		X	
379RC1-5B	X			
379RC1-6A	X		X	
379RC1-6B	X			
379RC1-10A	X			X
379RC1-10B	X			
379RC1-11A	X			X
379RC1-11B	X			
SF1-1B	X		X	X
SF1-2A	X		X	X
SF1-2B	X			
SF1-2C	X	X	X	X
SF1-3A	X		X	X
SF1-3B	X			
SF1-3C	X			
SF1-4A	X		X	X
SF1-4B	X			X
SF1-5A	X		X	X
SF1-5B	X			
SF1-5C	X			
SF1-6A	X		X	IRM
SF1-6B	X	X - failed	X - failed	X
SF1-7A	X			
SF1-8A	X		X	X
SF1-8B	X			
SF2-2A	X		X	X
SF2-2B	X	X - failed	X - failed	X
SF2-3A	X		X	X
SF2-3B	X			
SF2-3C	X			
SF2-4A	X		X	X
SF2-4B	X			
SF2-4C	X			
SF2-5A	X		X	X
SF2-5B	X	X	X	X
SF2-5C	X			
SF2-6A	X		X	X
SF2-6B	X			X
SF2-6C	X			
SF2-7A	X		X	IRM
SF2-7B	X		X	X
SF2-7C	X			
SF2-7D	X	X - failed	X - failed	X
SF2-8A	X			
SF2-9A	X		X	X
SF2-9B	X			X

SF2-9C	X		X	X
SF2-9D	X			
SF2-10A	X	X - failed	X - failed	X
SF2-10B	X			
SF2-10C	X			
SF2-10D	X			
SF2-11A	X		X	X
SF2-11B	X			
SF2-11C	X			
SF2-12A	X		X	X
SF2-12B	X			
SF2-12C	X			
SF2-12D	X		X	X

Thin Section Analysis
379RC1-3
379RC1-4
379RC1-7A
379RC1-9A
379RC1-7B
379RC1-8A
379RC1-8B
379RC1-9B
2_379RC1-1
2_379RC1-2
2_379RC1-7
2_379RC1-8
SF1-2B
SF1-3C
SF1-5C
SF2-3C
SF2-4C
SF2-5C
SF2-6C
SF2-10C
SF2-12C
SF2-8A